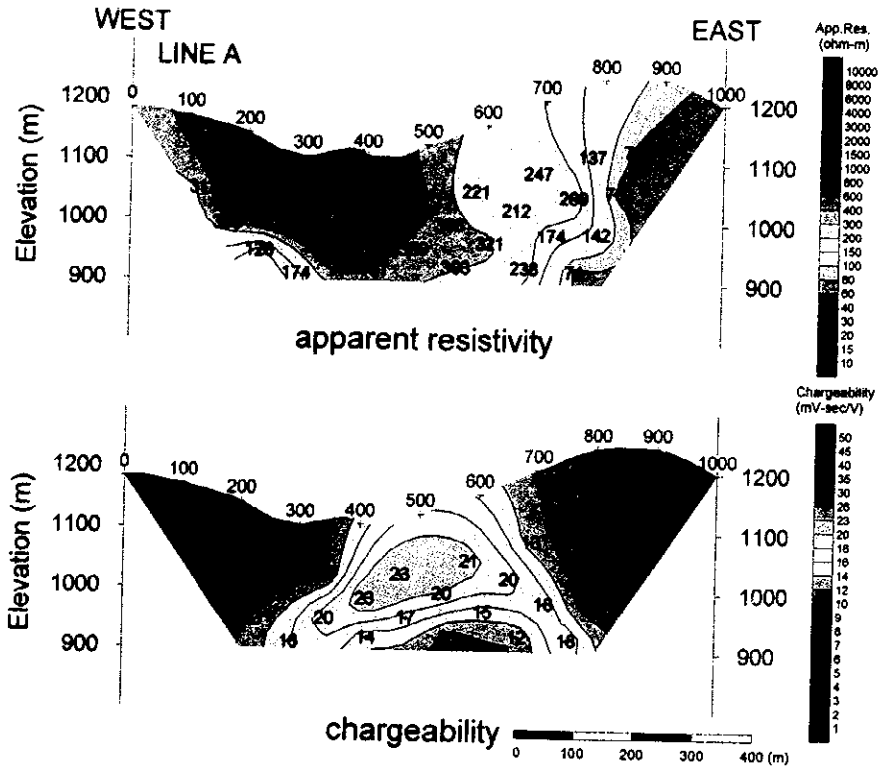

Fig.II-2-17 Pseudosection of apparent resistivity and chargeability of the Dong Noi area(A)

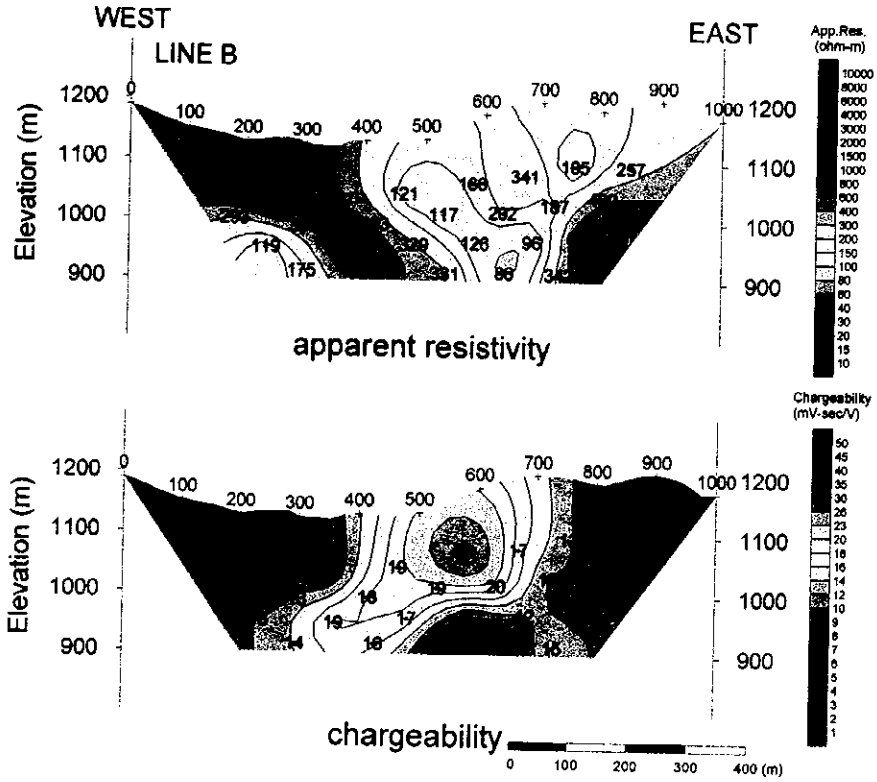

Fig.II-2-18 Pseudosection of apparent resistivity and chargeability of the Dong Noi area(B)

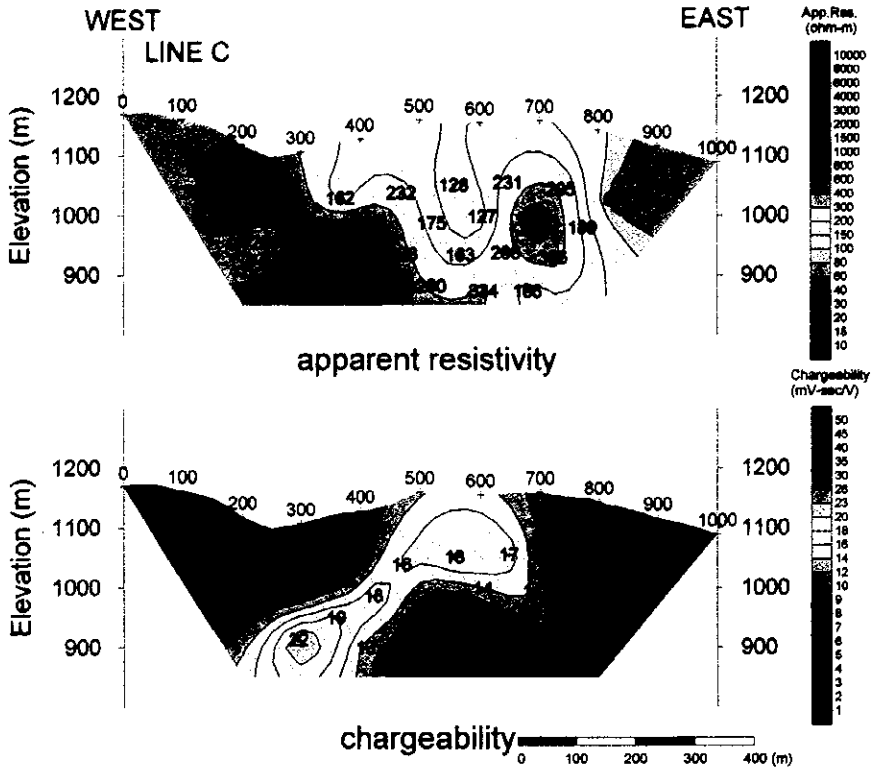

Fig.II-2-19 Pseudosection of apparent resistivity and chargeability of the Dong Noi area(C)

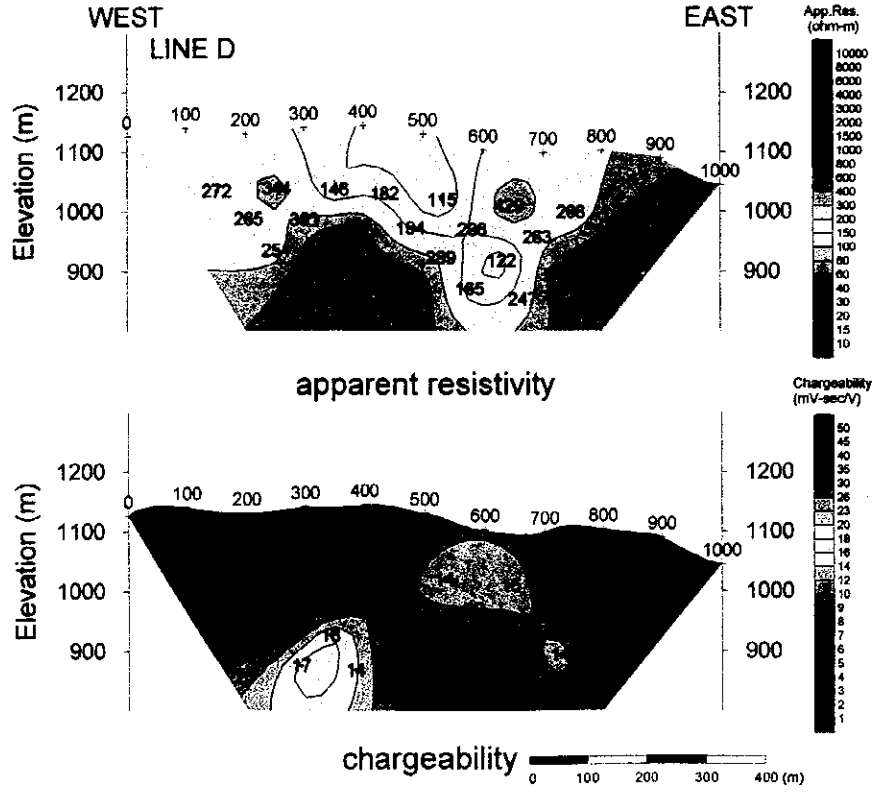

Fig.II-2-20 Pseudosection of apparent resistivity and chargeability of the Dong Noi area(D)

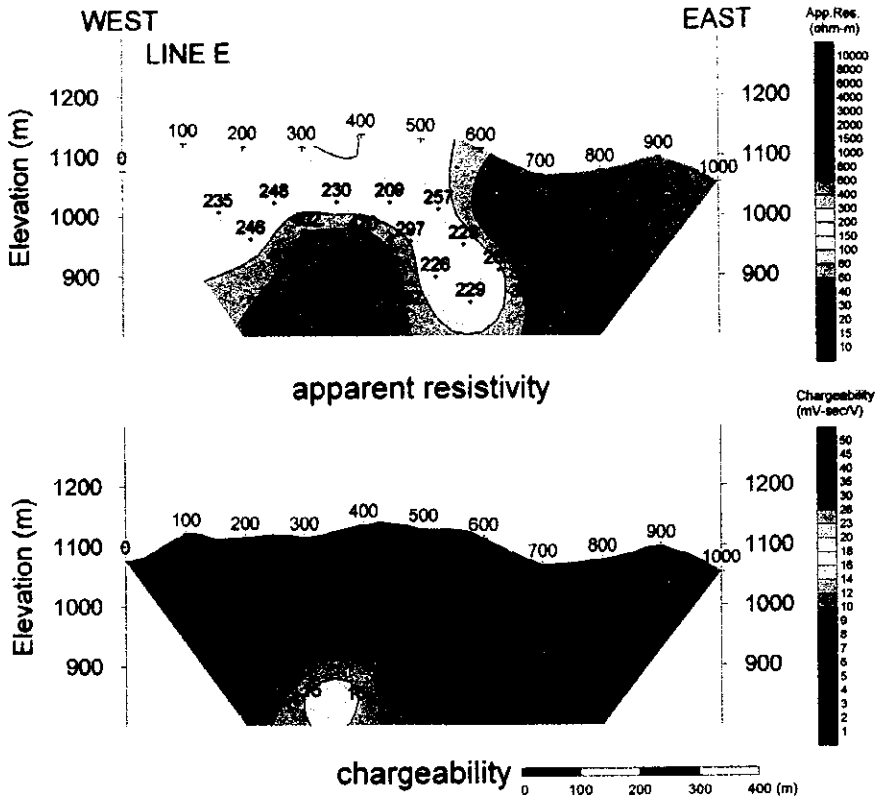

Fig.II-2-21 Pseudosection of apparent resistivity and chargeability of the Dong Noi area(E)

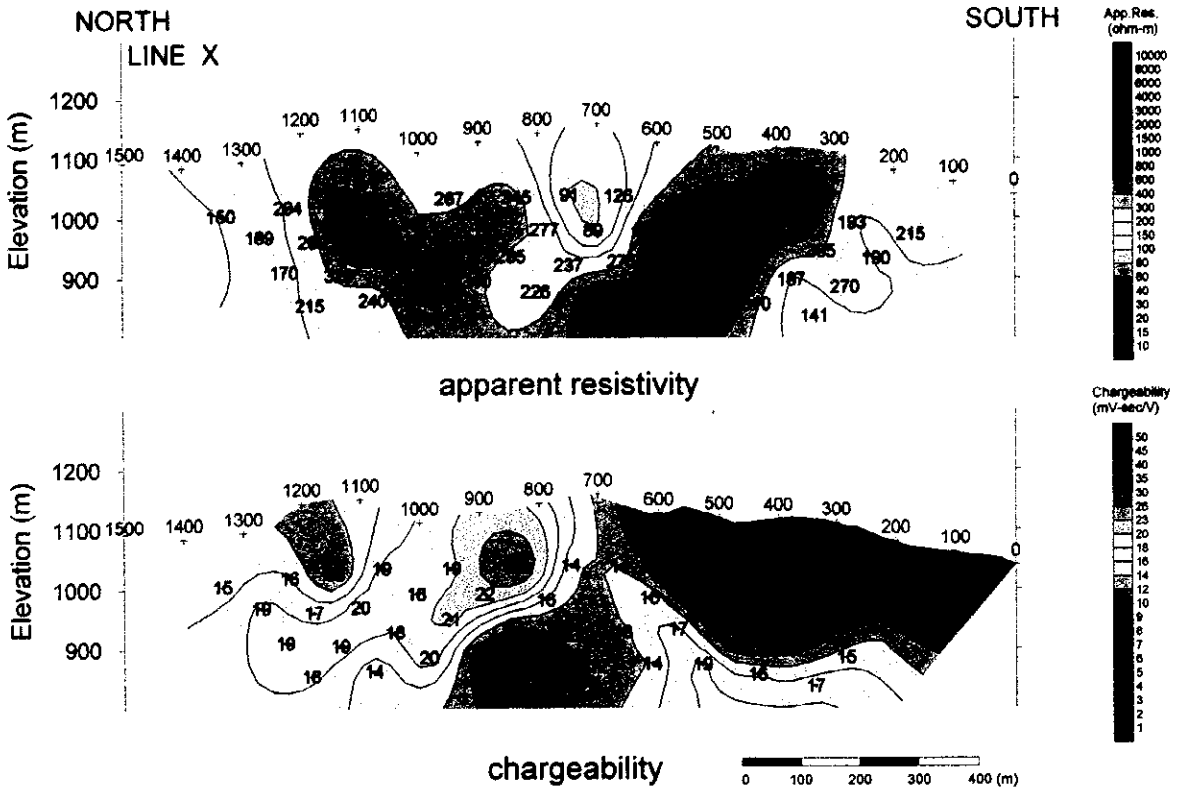

Fig.II-2-22 Pseudosection of apparent resistivity and chargeability of the Dong Noi area(X)

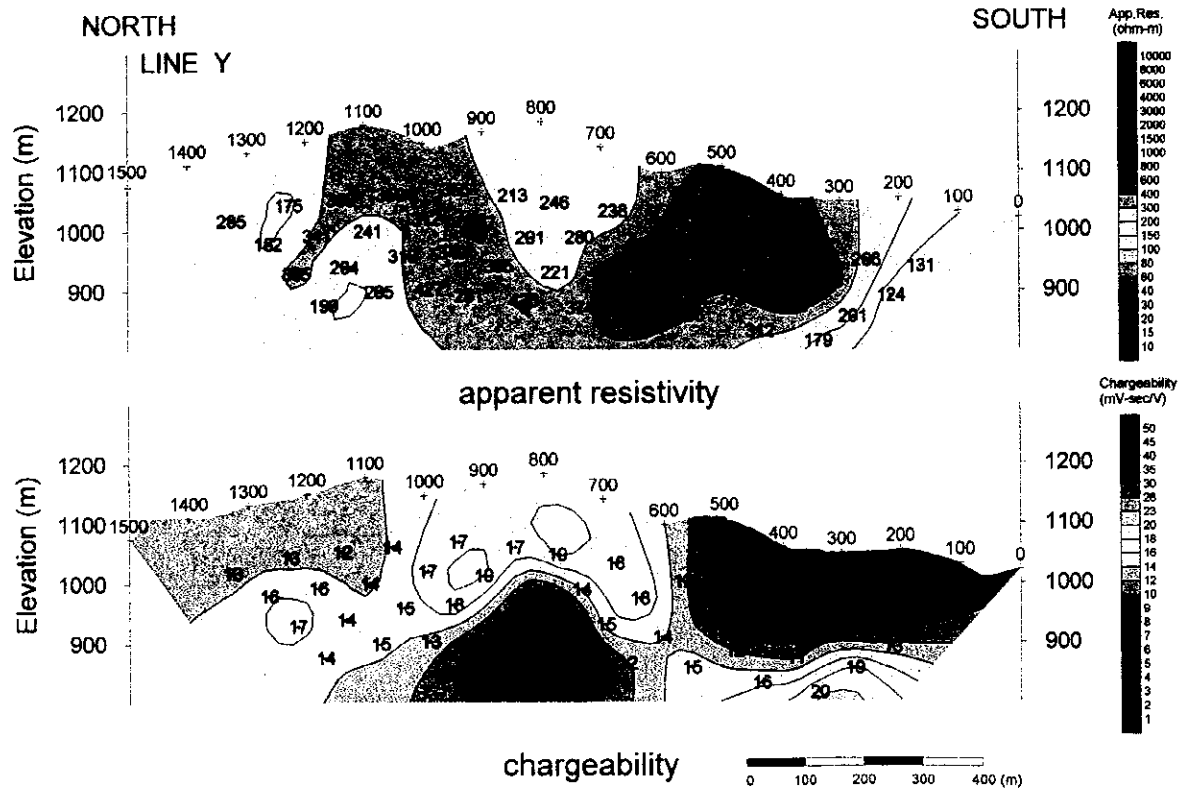

Fig.II-2-23 Pseudosection of apparent resistivity and chargeability of the Dong Noi area(Y)

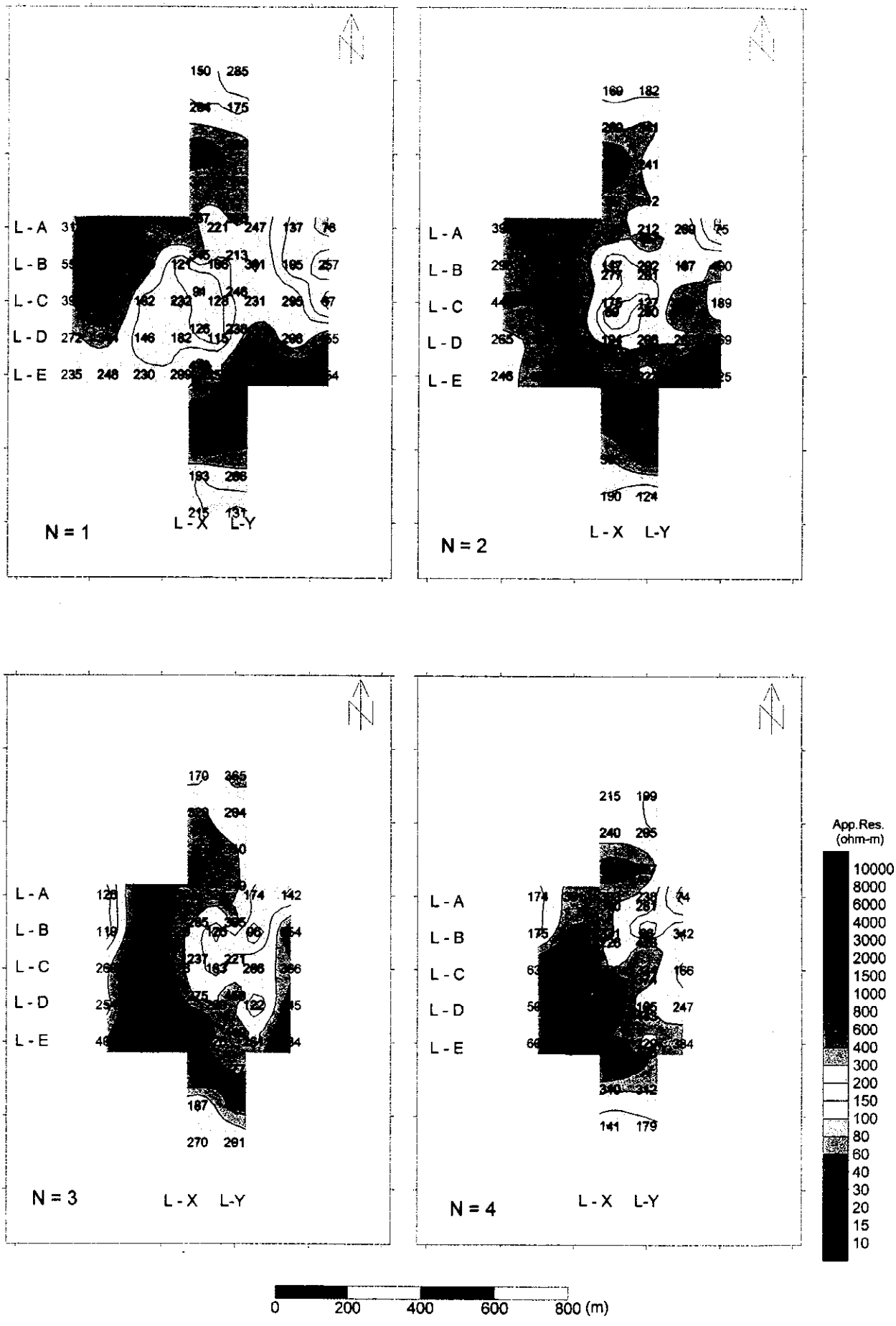

Fig.II-2-24 Plan map of apparent resistivity of the Dong Noi area

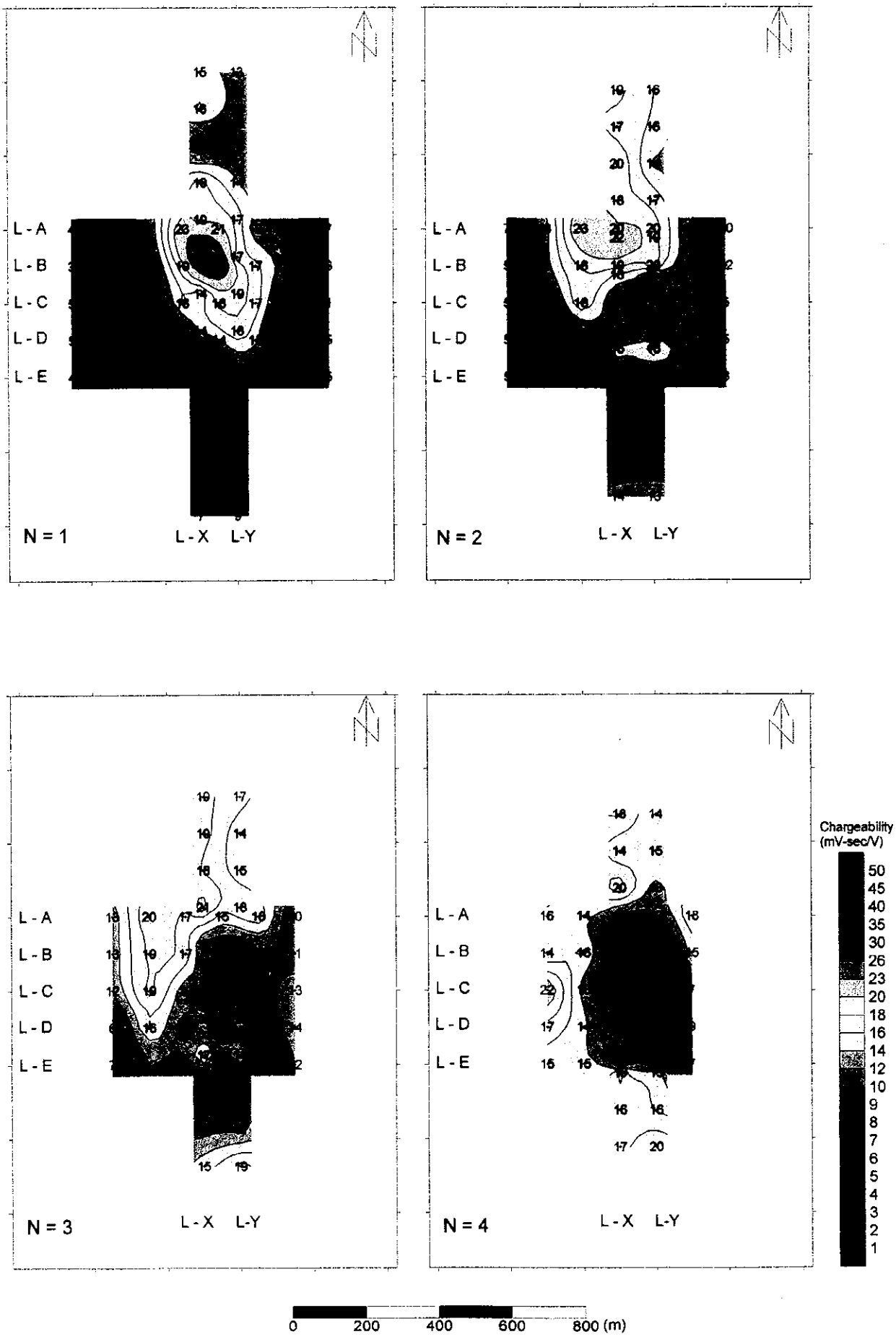

Fig.II-2-25 Plan map of chargeability of the Dong Noi area

The apparent resistivity shows from 124 Ω·m to 653 Ω·m value. The distribution of the apparent resistivity of less than 200 Ω·m is a little seen by the southern end of the line and the northern end part. The tendency of contour resembles line X, the apparent resistivity about 200Ω·m is distributed over the line center part and the apparent resistivity from 300Ω·m to 500 Ω·m are distributed over the part of the neighborhood of it.

Chargeability part a little less than 20mV·sec/V is observed from station 800 to 900 and the chargeability of convex type is being approximately distributed mainly in this . Also, the depth of station 300 shows the high chargeability of 20mV·sec/V but for the depth, the distribution situation is obscure.

8) Apparent resistivity plan map (Fig. II-2-24)

When seeing the result of N=1, the apparent resistivity of less than 200 Ω·m is distributed over the center part and the eastern end part of the area .It is narrowing the distribution range of a low apparent resistivity part in the center area as the depth increases (N becomes big). The low apparent resistivity part located in the eastern area is the end of line, so the situation (distribution and depth) is obscure. Incidentally, it is small, but the distribution of the apparent resistivity of less than 200 Ω·m is observed in the northern end part and the southern end part.

9) Chargeability plan map (Fig. II-2-25)

It finds that the high chargeability part which shows above 20mV·sec/V mainly in the neighborhood of station 500 of line B is spreading to line A when seeing the result of N=1. Also, when taking notice of the contour lines of 15mV·sec/V in near station 500 of line B, clearly finds that contour lines are spreading to the northern northwest - the southern southeast direction. The distribution of the high chargeability which shows above 20mV·sec/V rather shifts with the line A coming in N=2 . In N=3 and N=4, the chargeability value under about station 500 of line B falls (about 10) and high chargeability is observed in the part of the neighborhood of it. Also, N=4 can see a high chargeability station under about station 300 of line C and about station 300 of line Y.

2-6-5 Analysis results of 2-D

1) Line A (Fig. II-2-26)

The low resistivity zone of less than 200 Ω·m is distributed over the eastern side of the line. High resistivity zone is mainly distributed on the western side and the resistivity distribution area of more than 1000 Ω·m is seen to the shallowness between station 200 and 300.

As for the chargeability, high chargeability zone above 20mV·sec/V is seen around 1000m above the sea between station 400 and 600.

2) Line B (Fig. II-2-27)

As for the neighborhood of station 500 in the center of the line , the low resistivity zone of less than 200 Ω·m is distributed to the depth part. Also, the low resistivity zone of less than 200 Ω·m is seen to the shallowness of station 800, too.

The high resistivity zone is distributed as it puts in low resistivity zone in the center of the line and the high resistivity zone of more than 1000 Ω·m is seen to the station 200 shallowness.

As for the chargeability, high chargeability zone above 20mV·sec/V is seen from the shallowness to 1000m above the sea around station 500 and 600 .

3) Line C (Fig. II-2-28)

The low resistivity distribution area of less than 200 Ω·m is seen to the shallowness around stations 400 and 500, the shallowness of station 700 and the depth of eastern side of station 700 . The resistivity of another part of the line is relatively high and in the border in station 600 ,the eastern side shows around 300 Ω·m and the western side shows above 300 Ω·m.

High chargeability zone above 20mV·sec/V is seen around station 500 partially from the shallowness to 1100m above the sea .Contour line continues to the depth of the western side while it lowers a value.

4) Line D (Fig. II-2-29)

The low resistivity distribution area of less than 200 Ω·m is seen to the shallowness between stations 300 and 500. There are many parts which show the resistivity of more than 300 Ω·m in the other area.

As for the chargeability, high chargeability zone above 20mV·sec/V is seen around the 1000 m above the sea of station 500 partially. Also, while lowering a value like line D, contour line continues to the depth of western side .

5) Line E (Fig. II-2-30)

The low resistivity distribution area of less than 200 Ω·m is seen a little to the shallowness between station 300 and 400. Also, the high resistivity distribution area of more than 1000 Ω·m is seen around the 1000m above the sea below station 300 and around the 1000m above the sea below station 900.

As for the chargeability, a high chargeability part above 20mV·sec/V is seen around the 900m above the sea between station 100 and 500. It thinks that chargeability of this part indicated higher value than the measurement value because the resistivity of the high chargeability area was analyzed higher than the measurement value with actuality in the part of the neighborhood of the above the sea of 1000m between station 100 and 400.

6) Line X (Fig. II-2-31)

The low resistivity zone of less than 200 Ω·m is seen under station 100, in the shallowness between station 500 and 600, around the 900m above the sea between station 700 and 800, in the shallowness between station 800 and 900 and under about station 1400. As for the part

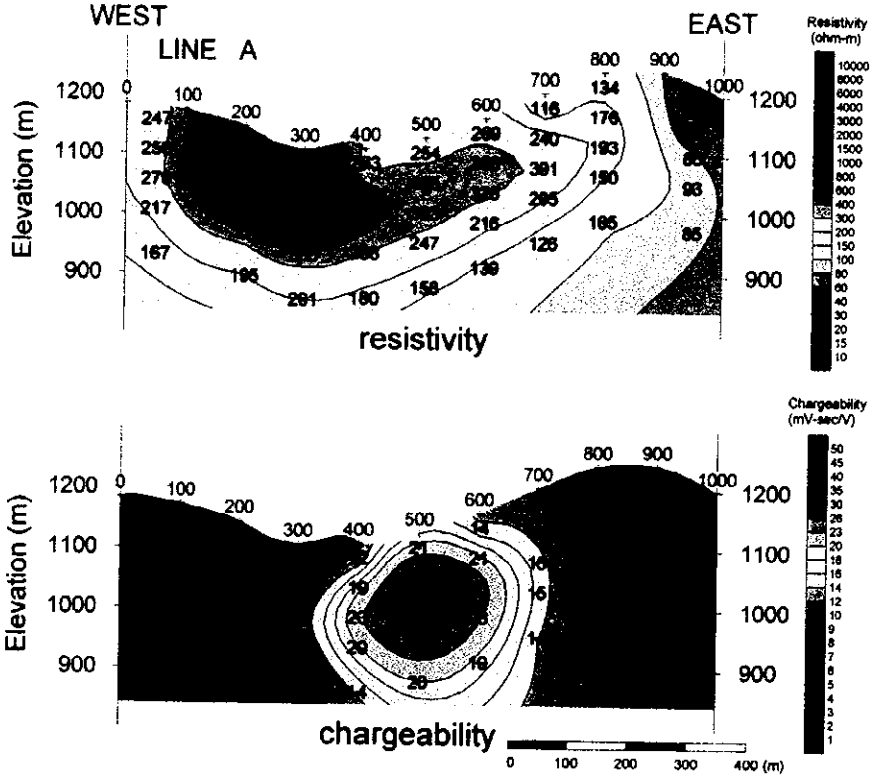

Fig.II-2-26 Results of model simulation of the Dong Noi area(A)

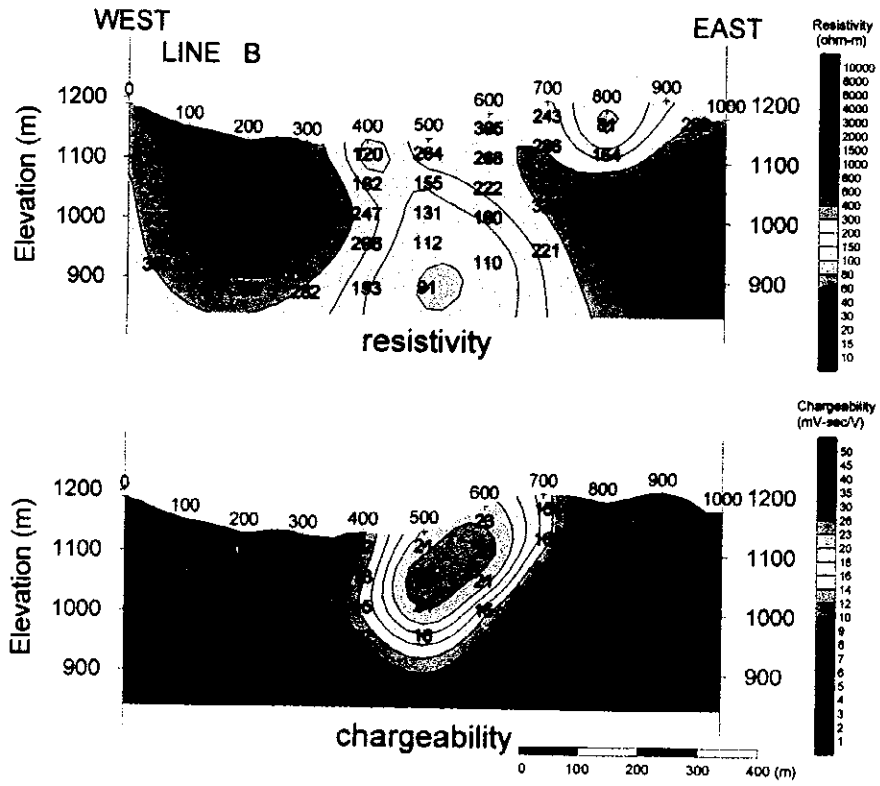

Fig. II-2-27 Results of model simulation of the Dong Noi area(B)

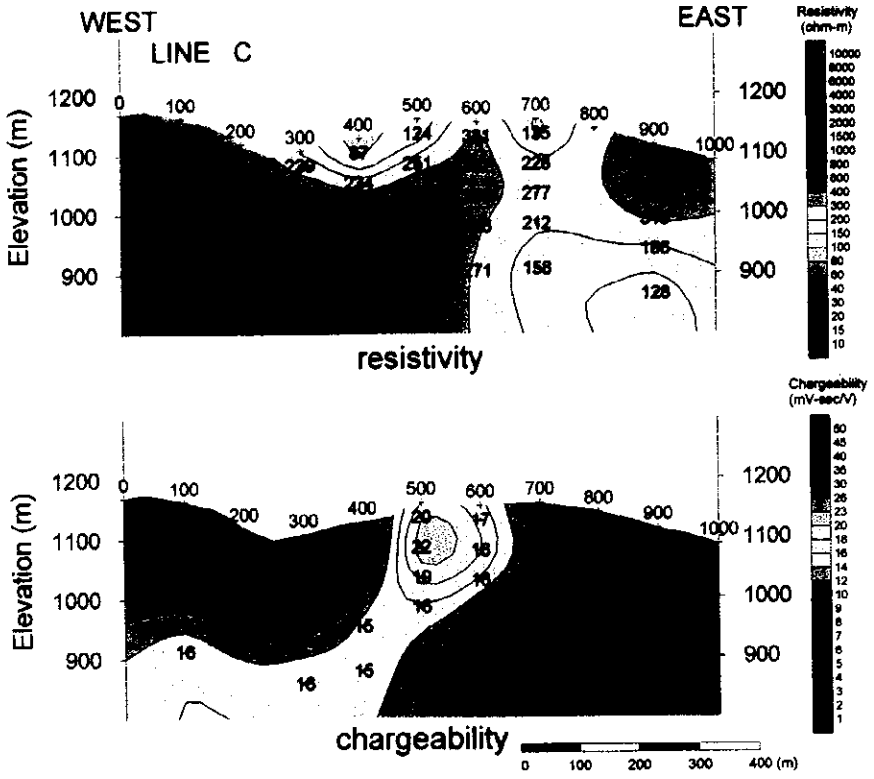

Fig.II-2-28 Results of model simulation of the Dong Noi area(C)

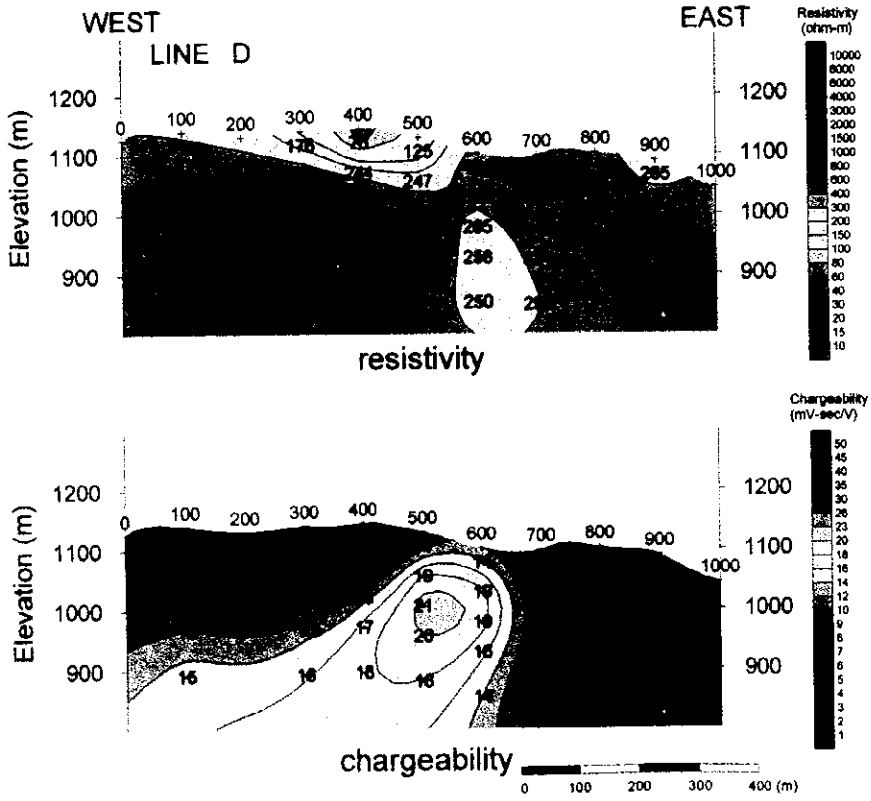

Fig.II-2-29 Results of model simulation of the Dong Noi area(D)

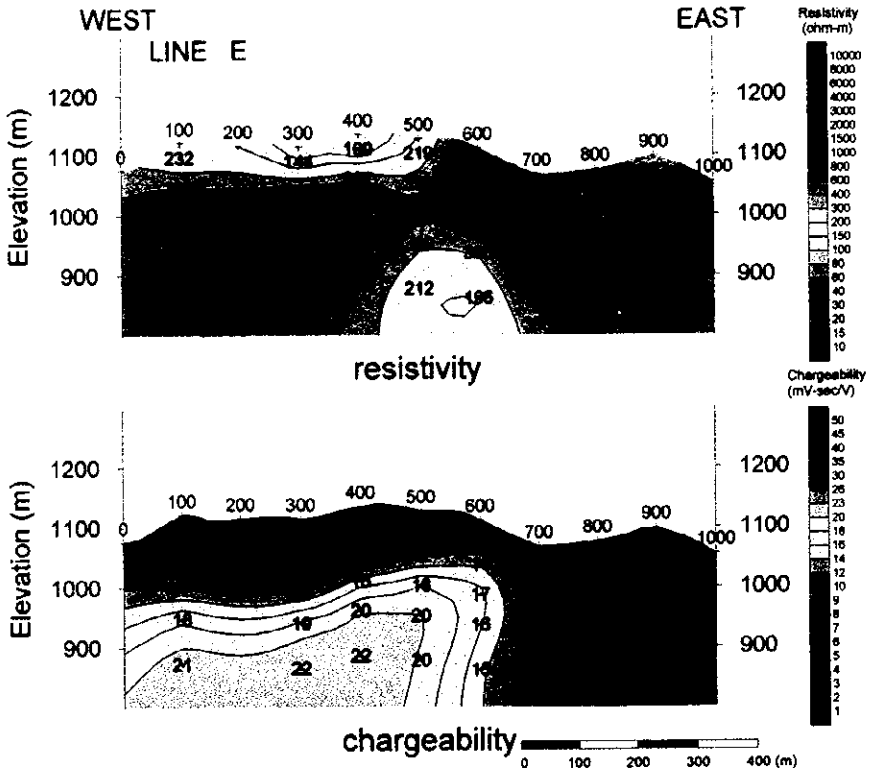

Fig.II-2-30 Results of model simulation of the Dong Noi area(E)

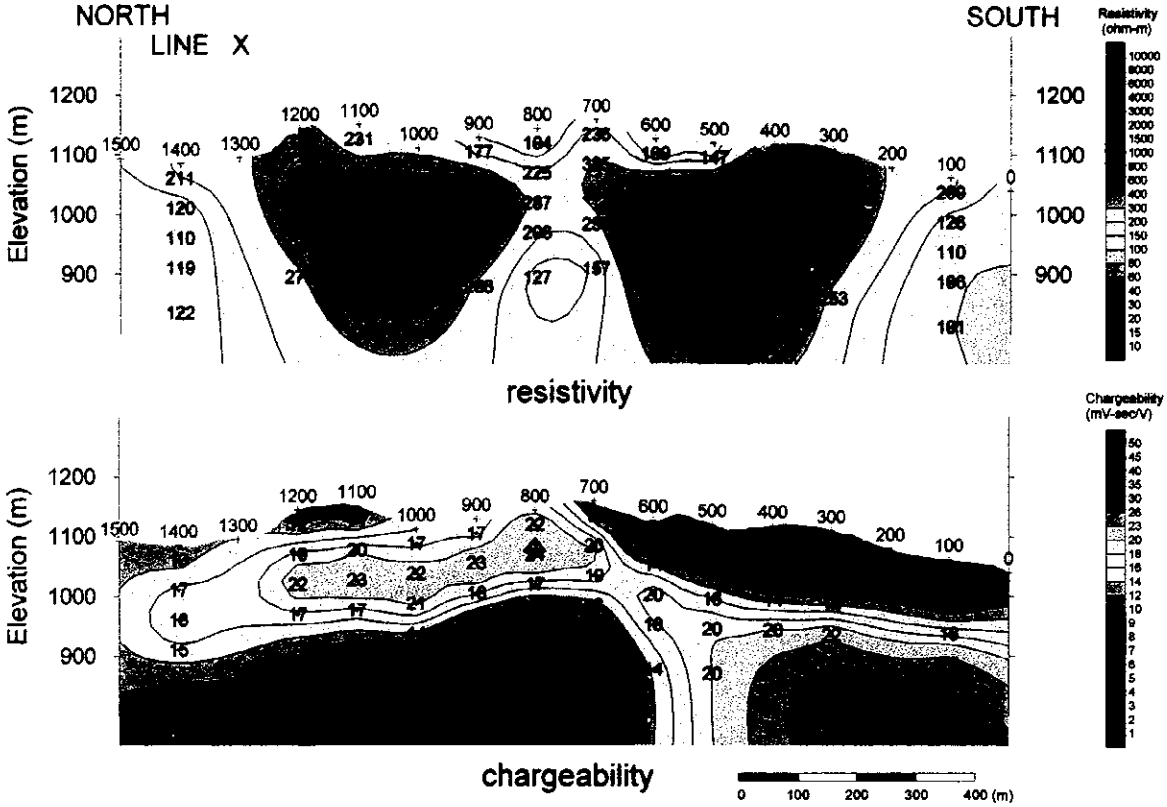

Fig.II-2-31 Results of model simulation of the Dong Noi area(X)

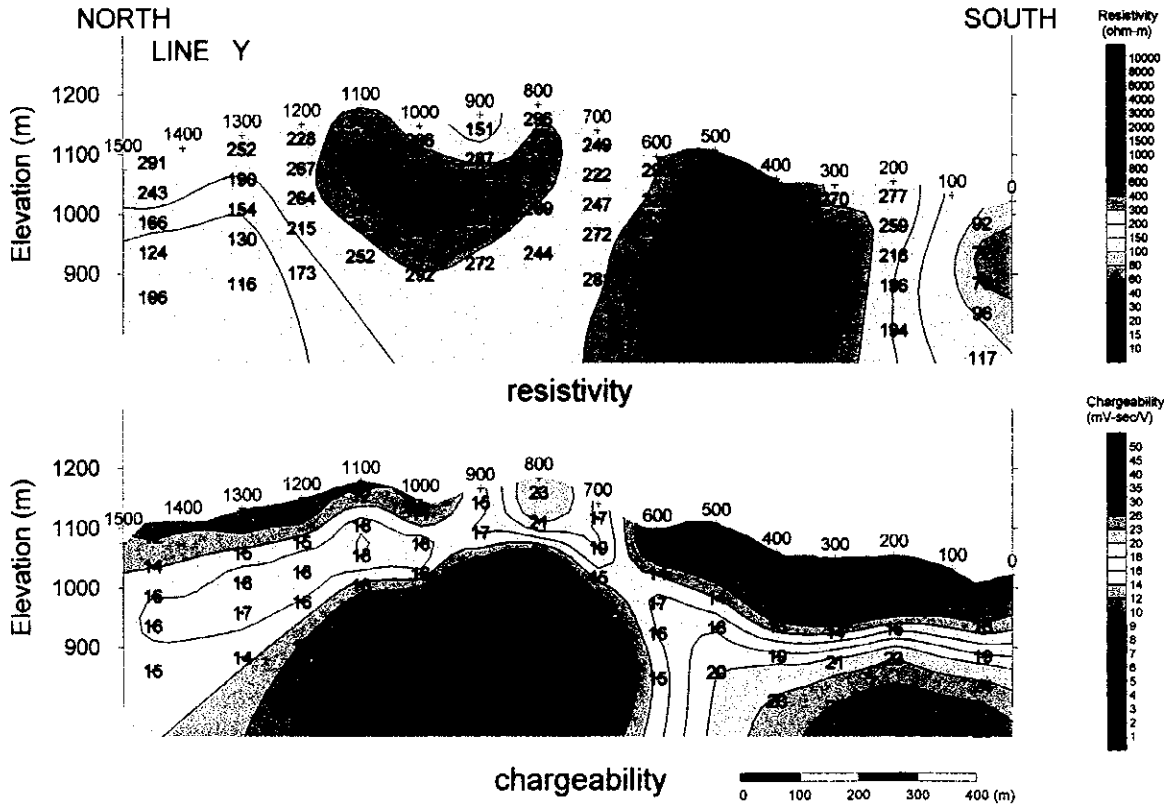

Fig.II-2-32 Results of model simulation of the Dong Noi area(Y)

except the low resistivity zone , high resistivity is distributed and especially at the about 1000m above the sea between station 400 and 600, the high resistivity zone of more than 1000 Ω·m is analyzed. Incidentally, the distribution of this high resistivity does not continue under station 700.

As for the chargeability, high chargeability above 20mV·sec/V is ranged from the shallowness to the 1000m above the sea between station 700 and 1200. Also, a high chargeability part above 20mV·sec/V is seen in the southern part from station 600 around 900m and 1000m above the sea . Because the increased resistivity zone of more than 1000 Ω·m was analyzed in the same way as line E from the measurement value by the around 1000m above the sea between station 400 and 600, it thinks that chargeability, too, was calculated higher.

7) Line Y (Fig. Ⅱ-2-32)

The low resistivity zone of less than 200 Ω·m is seen around the south end of the line, the shallowness of station 900 and around the 1000m above the sea of the north from station 1300 . As for the other part, resistivity ranged from 200Ω·m to 300 Ω·m ,lower then line X ,is widely distributed . And at the station 700 the resistivity value of the southern part and the northern part is different and some un-continuing structure is estimated by this part.

As for the chargeability, high chargeability above 20mV·sec/V is seen to the shallowness of station 800. Also, a high chargeability part above 20mV·sec/V is seen from 900m above the sea to the depth between station 0 and 500. Because the resistivity of increase was analyzed in the same situation as line E·X from the measurement value by the about 1000m above the sea between station 400 and 600, it thinks that chargeability, too, was calculated to raise.

2-6-6 Discussion

Apparent resistivity in this area is distributed from 67Ω·m to 1608 Ω·m and the chargeability shows a maximum of 28 mV·sec/V.

It extracted the part which shows the apparent resistivity of less than 200 Ω·m from the result of N=1 of the IP method measurement in Fig. Ⅱ-2-33 and the part which shows high chargeability above 20mV·sec/V. Also, faults and ore bearing places was shown all together, pulling out from the geological map.

The ore bearing place is located in station 500 of line C. The apparent resistivity in this spot is about 100 Ω·m and the chargeability is 18 mV·sec/V ,rather high value .

Also, the sample which shows the chargeability 18mV·sec/V is seen by the rock sample (containing galena) which was gathered around this station. According to the geological survey result, around this ore bearing place, the distribution of galena is seen. And the fault that run east and west approximately according to line D to the side of its south and the fault that run north and south is running to the eastern side.

The low apparent resistivity of less than 200 Ω·m is distributed around the end of north

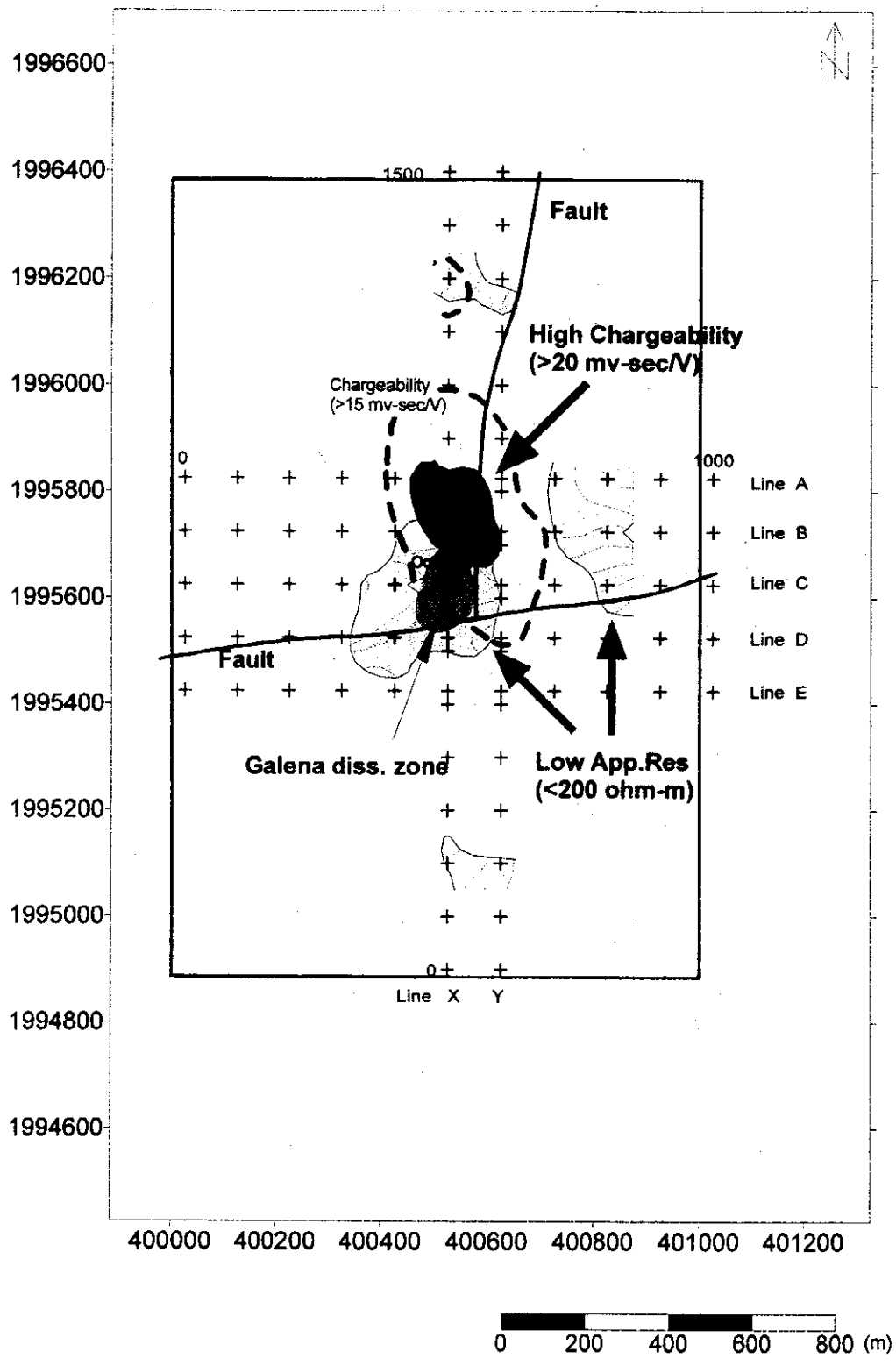

Fig.II-2-33 Integrated plan map of the Dong Noi area

and south in the area, the part of the end of the east and above-mentioned ore bearing place (the area center part).The part shows high chargeability is distributed as it is seen along the fault that run north and south and comes in touch with the low apparent resistivity distribution of the center part of the area. In this way, as for the neighborhood of the ore bearing place which is located in station 500 of line C, near the non- continuation part of the underground structure, a lot of anomalies by the geophysical exploration result are observed.

In Fig. Ⅱ-2-33 , from the chargeability plan map of N=1 ,it is displaying contour of 15 mV·sec/V by the pulling-out dotted line . When seeing this, this area shows one with the distribution tendency with chargeability in the NNW – SSE .It thinks that this direction is the tendency that is related with the underground structure of this area in the commonness to the geochemical prospecting result, too.

Next, it examines about the relation between the analysis result of 2-D and the fault.

In line X·Y, the continue-ability of the high resistivity breaks off under station 600 and 700. It thinks that this position is the place where the fault that run east and west and line X·Y intersect ,so the discontinuation part which is seen by this line X·Y shows this fault. Also, when seeing the chargeability of the north of station 700 , the chargeability of the place around 20 mV·sec/V is distributed but this is supposed whether or not to be because a ore bearing zone is distributed along the fault that run north and south. Also, for the depth of the south part of the line from the depth in station 600, the distribution of the chargeability of the place around 20 mV·sec/V is seen, but is situated on the part of the end of line and the details are obscure.

When seeing the 2-D analysis result of line B·C, the tendency of the resistivity is rather different at the border in station 500 or 600 ,but it thinks that this is the change which corresponded to the fault that run north and south. Especially, the low resistivity of less than 200 Ω·m is widely distributed over line B under station 500 and 600 where the fault intersects. Incidentally, because of the fault that run north and south and because line D·E doesn't intersect, at the shallowness near station 600, the discontinuation of the resistivity isn't observed at the line D·E.

As the anomaly area by the geophysical exploration result in the Dong Noi area, the area which spreads around station 500 and 600 from line B to line D which hits a ore bearing place is extracted from above result. It is very interesting that the distribution area of the low resistivity is big in B line result of the pseudo section and the analysis result of 2-D .

Also, because the chargeability of the high values is distributed about the southern part of line X·Y, too, and attracts attention but an anomaly is rather seen to the depth, it is difficult to grasp the distribution situation.

2-7 General consideration

The Dong Noi area consists of the Cambrian and Ordovician sedimentary rocks. The area

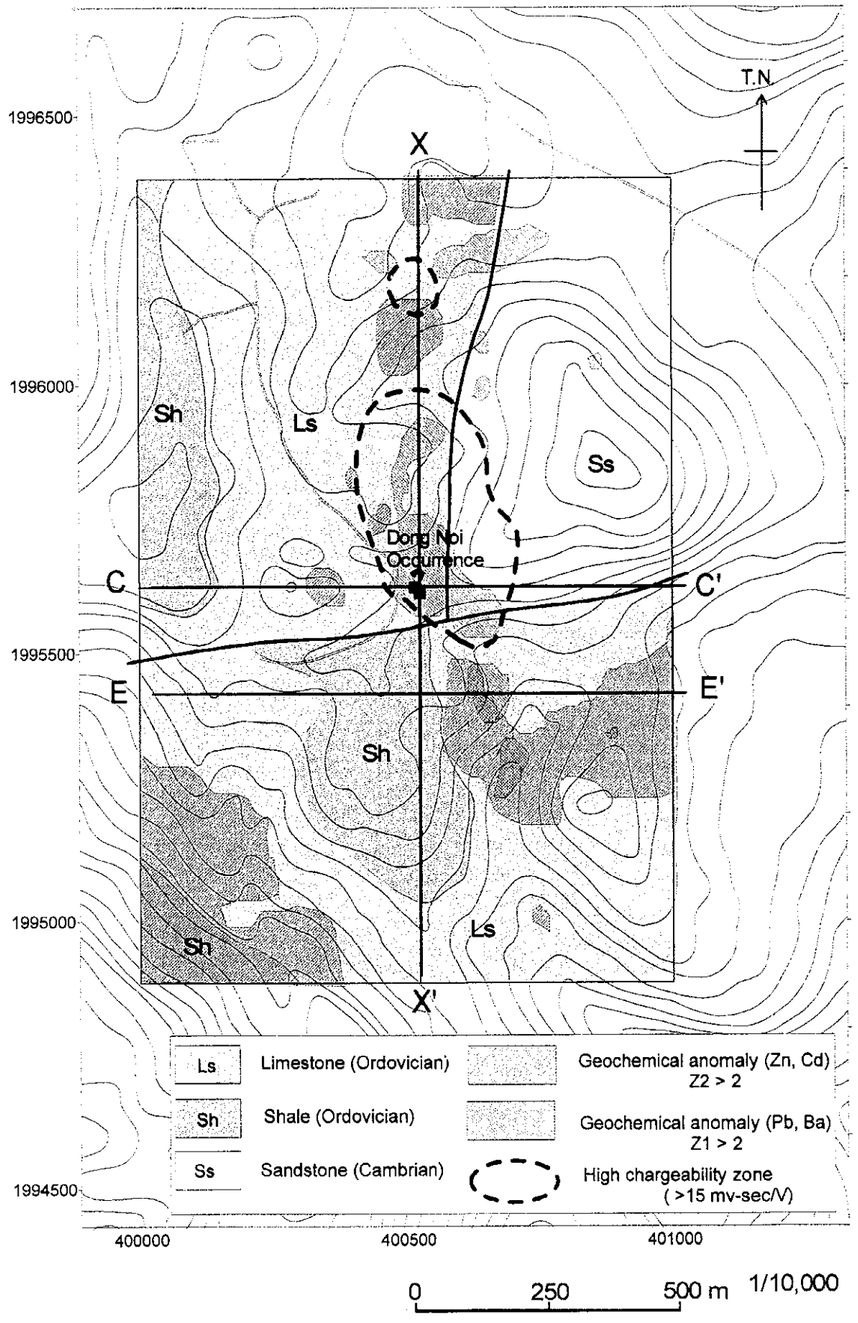

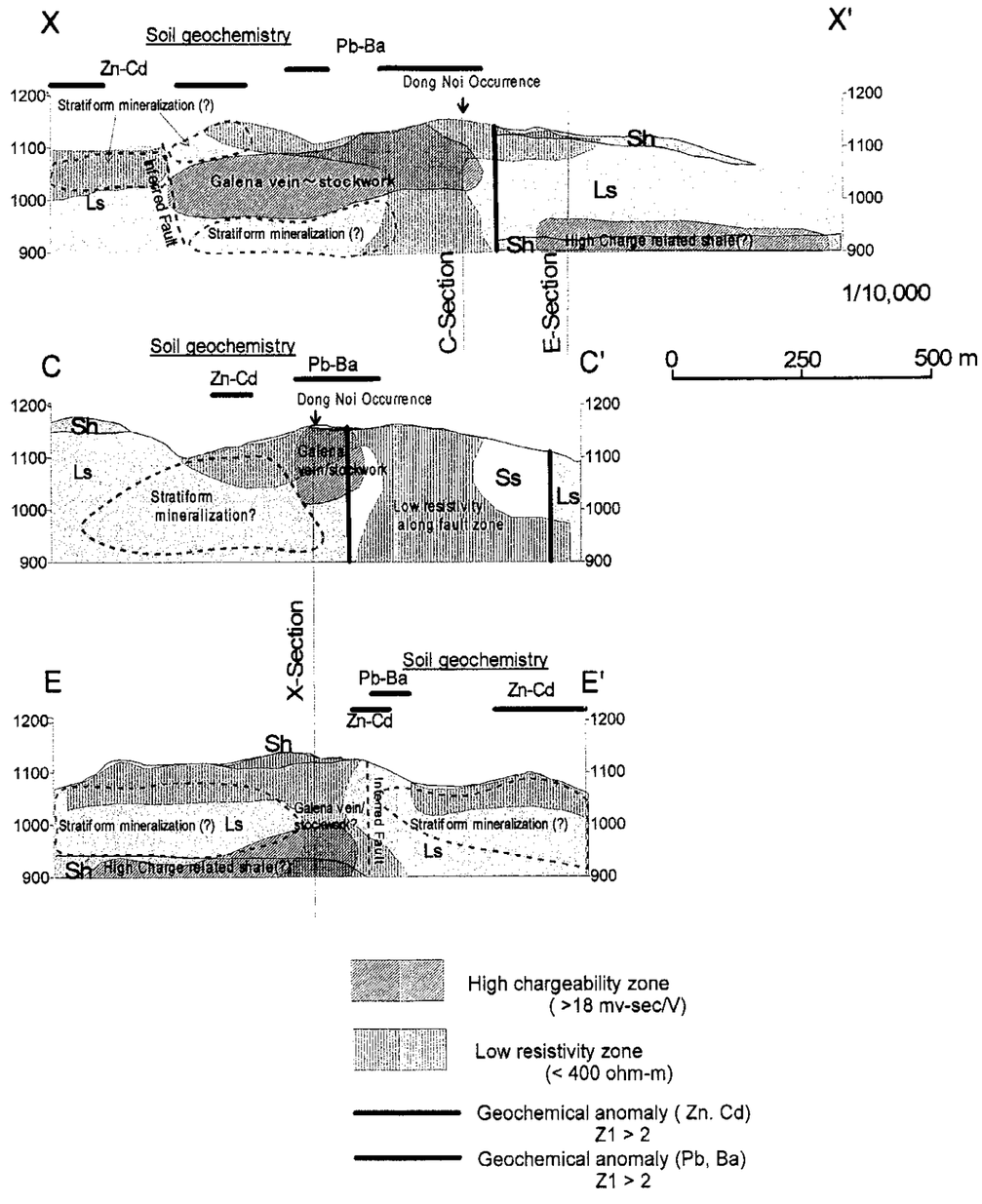

Fig.II-2-34 Interpretation map and profile of the Dong Noi area

is divided into northern and southern parts by a fault in the E-W direction. In the northern part the Ordovician sedimentary rocks and the Cambrian sandstone are distributed while the Cambrian sandstone is not distributed in the southern part. The northern part is divided into east and west by a fault in the north - south direction. The Cambrian outcrops in the eastern side and Ordovician limestone are distributed in the west side, respectively.

The Dong Noi area has a distribution of a galena-barite ore body in the north - south direction around a small hill in the center of the area, magnetite dissemination in the Cambrian sandstone, Gossan floats in the northern part of the area, etc. The galena - barite orebody shows a distribution spreading 100 m x 200 m long north and south including a distribution range of floats, which is assumed to be a mineralized zone predominated by a north - south fault. According to the ore assay results, 3.4 to 14.8 % of Pb, 58 to 146 g/t of Ag were obtained, but the concentrations of other elements are not so high. At test pit No.2 in the 40m east of the outcrop, 970 ppm of Cu and 32.4 g/t of Ag were obtained.

The geochemical survey revealed that a geochemical anomaly of Pb, Ba, Fe, and Mn is distributed in the NNW to SSE directions from the above orebody outcrop. An extension of an anomaly is greater to the northern part. On the other hand, it disappears immediately beyond the east - west fault in the southern part. The first principal component is considered to be a factor representing this mineralization. A combination of elements Pb, Ba, Sb, and Cu is the same combination of elements in a galena - barite - quartz vein often observed in the Mae Sariang area. It is considered that such a mineralization represents a possibility of an existence of vein-type mineralization zone.

The score distribution of the first principal component shows that the mineralization mainly spreads in the NNW - SSE direction from the orebody outcrop and branches and crosses in the east - west direction along a east - west fracture in the northernmost part. It is thought that this is an orebody formed by an ore solution which caused a mineralization of Pb and Ba along the north - south fault and in part along the east - west derived fault.

A subsurface high chargeability zone at survey points from 700 to 1400 of traverse lines X and Y and survey points from 400 to 600 of traverse lines A and B in the IP exploration results shows that this mineralized zone exists under the ground. An orebody at the outcrop is strongly silicified and exceedingly heterogeneous and the amount of galena remarkably varies. For this reason, chargeability values in a property test, 1.4 to 18.8 mV/sec/V, has a big difference depend on proportion of the ratio of galena in quantity. A chargeability beneath the orebody outcrop in the model simulation is about 20 mV·sec/V, which almost coincides with the highest value among the property test values. On the other hand, a high chargeability zone further north from this indicates a high value of 20 to 32 mV·sec/V. This fact indicates an existence of a mineralized zone accompanies by galena or other sulfide minerals having a grade higher than the outcrop.

It is a possibility that high chargeability zones observed at survey points from 0 to 500 of

IP traverse lines C, D, and E below 950 m above sea level and in depths on the south side along traverse lines X and Y may be an orebody. However, since the geological situation shows a coincidence with the distribution of shale of the lower Ordovician system, this is judged as a high chargeability zone formed by shale layer.

The Zn geochemical anomaly is accompanied by Cd, Mg, and Mn anomaly and overlaps the Ordovician limestone area in the southeastern part and that ranging from the southwestern part to the southern part of the area. In the neighborhood coarse grain recrystalline limestone is exposed and no special ore showing is observed with the naked eye. The Mae Sod Mine of Padeang Industry is a zinc deposit which replaced limestone and this deposit is characterized by the fact that it brought about dolomitization and magnesitization in limestone of country rock and it is accompanied by Cd. The Zn geochemical anomaly in the Dong Noi area is similar to the mineralization of this Padeang Mine, which indicates a possibility that a stratiform deposit replacing limestone of the same type will exist. This Zn geochemical anomaly zone exists in limestone so that it does not indicate a remarkably low specific resistance and the chargeability is also very low. According to traverse line E of the IP exploration, it is thought that the distribution of a weathered shale at the surface also has an influence upon this anomaly area on the western side. A relatively low specific resistibity area stretches in correspondence with the Zn anomaly area and this probably indicates a mineralized zone.

According to cross sections of the IP traverse lines C, D, and E, an inferred fault is presumed near survey points 500 to 600. There is a strong possibility that a north - south fault in the northern part will continue in the southern part of the area. The appearance of chargeability in cross section differs in both side of this inferred fault. As mentioned above, supposing that a high chargeability zone in the depths on the west side indicates a shale layer, this shale layer is not distributed down to the bottommost depth of the cross section in the eastern part and a limestone layer thickness remarkably differs.

Considering that the Zn geochemical anomaly exists at almost the same altitude, it is thought that the Zn mineralization horizon is differed in the east and west side.

The mineralization in the Dong Noi area is considered as follows:

A mineralizing solution rising along the north-south fault formed a vein type or network orebody mainly composed of galena along the fault.

The mineralizing residual solution containing zinc and cadmium flows a specific horizon in limestone to one side and replaced limestone to form a stratiform ore body.

Chapter 3 Results of detailed survey in the I-4 area

3-1. Outline of geology

The I-4 area can be divided into two blocks, northwestern part and southeastern part, by a fault in the NE - SW direction located in the central part of the area. The northwestern part consists of the Ordovician sedimentary rocks and the southeastern part consists of the Permian Period to Triassic Period sedimentary rocks.

3-2. Details of geology

3-2-1. Ordovician sedimentary rocks

There are located in the southernmost part of Ordovician sedimentary rocks which continues more than 15 Km north and south from the neighborhood of Huai Hat Ta Lan in the middle north of the survey area. On the north side of Nam Mae Sariang, 700 to 900 m high mountains are formed. A limestone of the upper formation covers at the top of mountains. An lower alternation of shale and sandstone are distributed along Nam Mae Sariang, respectively.

There are cut by a fault in the NE - SW direction at the middle of the I-4 area. The lower formation appears in the eastern part and southwestern part and forms, as a whole, a synclinal structure like a ship bottom plunging on the north side.

The lower formation consists of alternating beds of foliated grayish black shale, reddish violet shale and fine grain sandstone, and medium to coarse grain sandstone.

The lower pat of limestone formation consists of alternating thin beds of limestone and pale green to pale brown siltstone. There are fewer partings upward, and grading into banded limestone containing a lot of pale gray to pale reddish violet impurities. This seems to be intercalating shale and sandstone layers on the west slope of the mountaintop, because there is no outcrop but small floats of mudstone and sandstone are distributed

The massive limestone is strongly foliated and a small-scale cockpit karst landform with a strong preferred orientation is formed by leaching and erosion along the foliation. In addition to veinlets of calcite developed in network form in the limestone, there are a lot of floats of recrystallized coarse grain calcite, etc.

3-2-2 Permian to Triassic sedimentary rocks

The Permian to Triassic sedimentary rocks, from the base upward, consist of alternating beds of sandstone and shale, and chert. The alternating beds of sandstone and mudstone are dominant in black shale intercalating pale gray sandstone rich in quartz. It contains small lenses of limestone in part and in its neighborhood the shale is also calcareous. The upper chert is hard and platy form with 2 cm width.

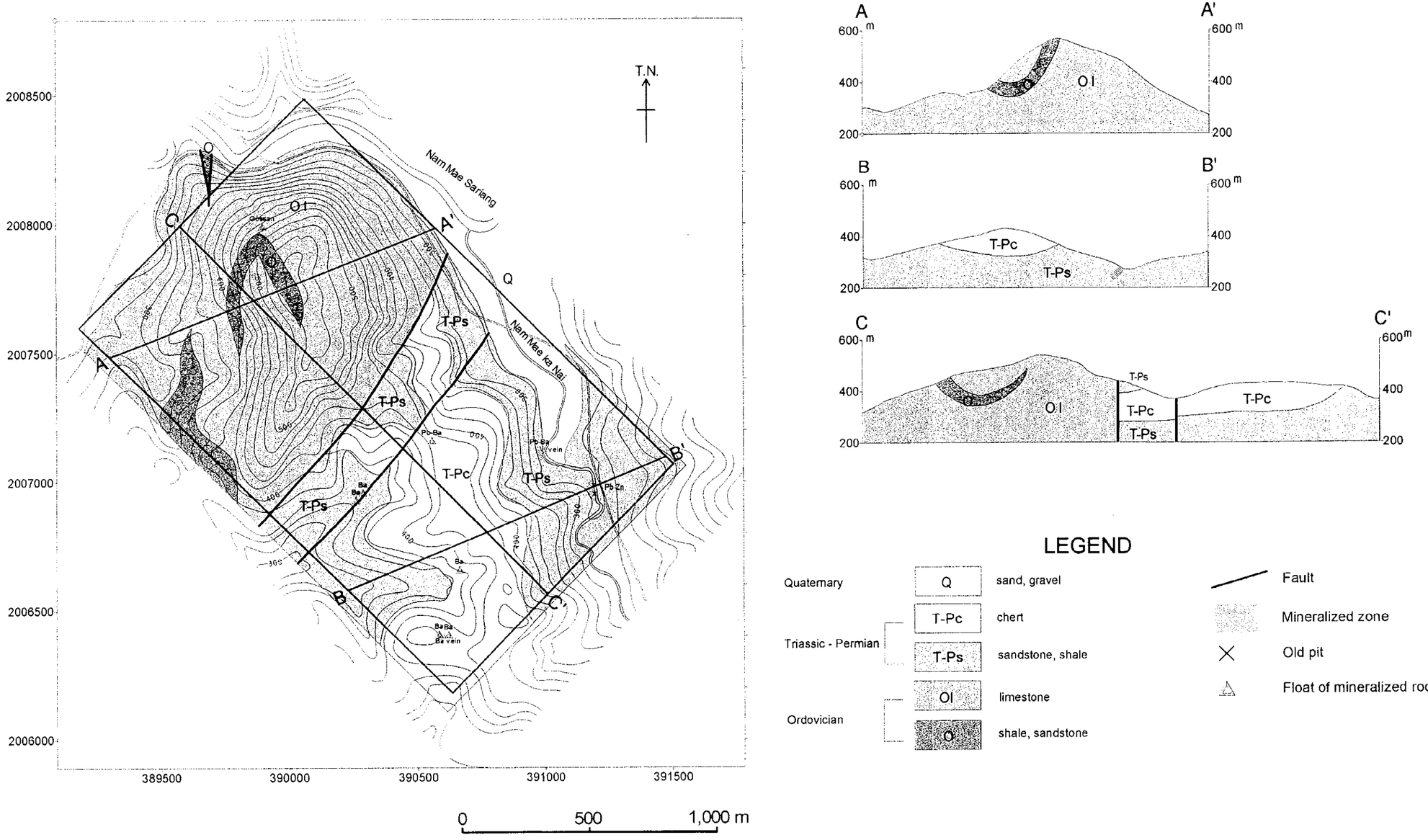

Fig.II-3-1 Geologic map and profile of the I-4 area

3-3. Geological structure

Not only the geological distribution but also the structure greatly differs due to a fault crossing the central part of the area in the northeast and southwest direction. The Permian to Triassic sedimentary rocks distributed in the southeastern part of the area show a strike from the north - south to slightly west and shows a monoclinal structure about 30 degrees on the west side. On the other hand, as mentioned above, the Ordovician delineated, as a whole, a synclinal structure like a ship bottom plunging north side. The overall structure is very complicate. Because in many cases, a small-scale folding structure is observed even in limestone outcrop and the foliation is well developed. A foliation of limestone strikes north to south slightly toward east and dips 80 to 90 ° toward both east and west.

3-4. Ore deposit and occurrences

A fluorite deposit occurs in the Ordovician limestone along the northern bank of Nam Mae Sariang, but no remarkable mineral showing is observed in the limestone within the I-4 area. Small gossan floats are observed in the neighborhood of a parting of mudstone and sandstone near the mountaintop. Also, many barren quartz vein floats are distributed at the foot of the mountain in the northern part of the area.

Floats of barite, galena-quartz vein, quartz vein, etc. are distributed here and there in the Permian to Triassic sedimentary rocks. In addition, a large amount of pyritic dissemination is observed on chert along a national highway at the east end of the area.

Strongly silicified shale crops out over 70 m north and south on the left bank of Nam Mae Ka Nai, a tributary of Nam Mae Sariang in the southwestern part of the I-4 area. A 10 to 15 m wide mineralized zone composed of galena - arsenopyrite - sphalerite are observed in three places on the north side, central part, and south side of this outcrop (Fig.II-3-2).

Bedded silicified rocks have a galena - arsenopyrite dissemination and a stockwork vein in a mineralized zone on the north and are characteristically accompanied by a large amount of tremolite as a gangue mineral. The full view is not known because the north end of the outcrop is covered by alluvial gravel. The width of mineralized zone is about 10 m even observably. The mineralized zone strikes N 55° W and dips 80° N. It is obviously concordant with silicified shale, country rocks, striking N 5° W and dipping 50° W. The amount ratio of sulfide in the mineralized zone is not uniform and there are some parts in which arsenopyrite concentrated in the direction of the mineralized zone looks like a band. Some of sulfide veins consist of only galena with a maximum vein width of about 20 cm. Rocks considered to be part of this mineralized zone containing a lot of veinlets of galena - arsenopyrite - sphalerite which look like silicified granite crop out 5 m north of this outcrop. The ore assay of the samples (AR010) taken from here revealed the presence of Pb of 8.15 % and Zn of 1.53 %.

A galena - arsenopyrite dissemination and a stockwork vein with a fault breccia zone having a strike of N 60° W and an inclination of 60° N inserted are observed on both sides in the

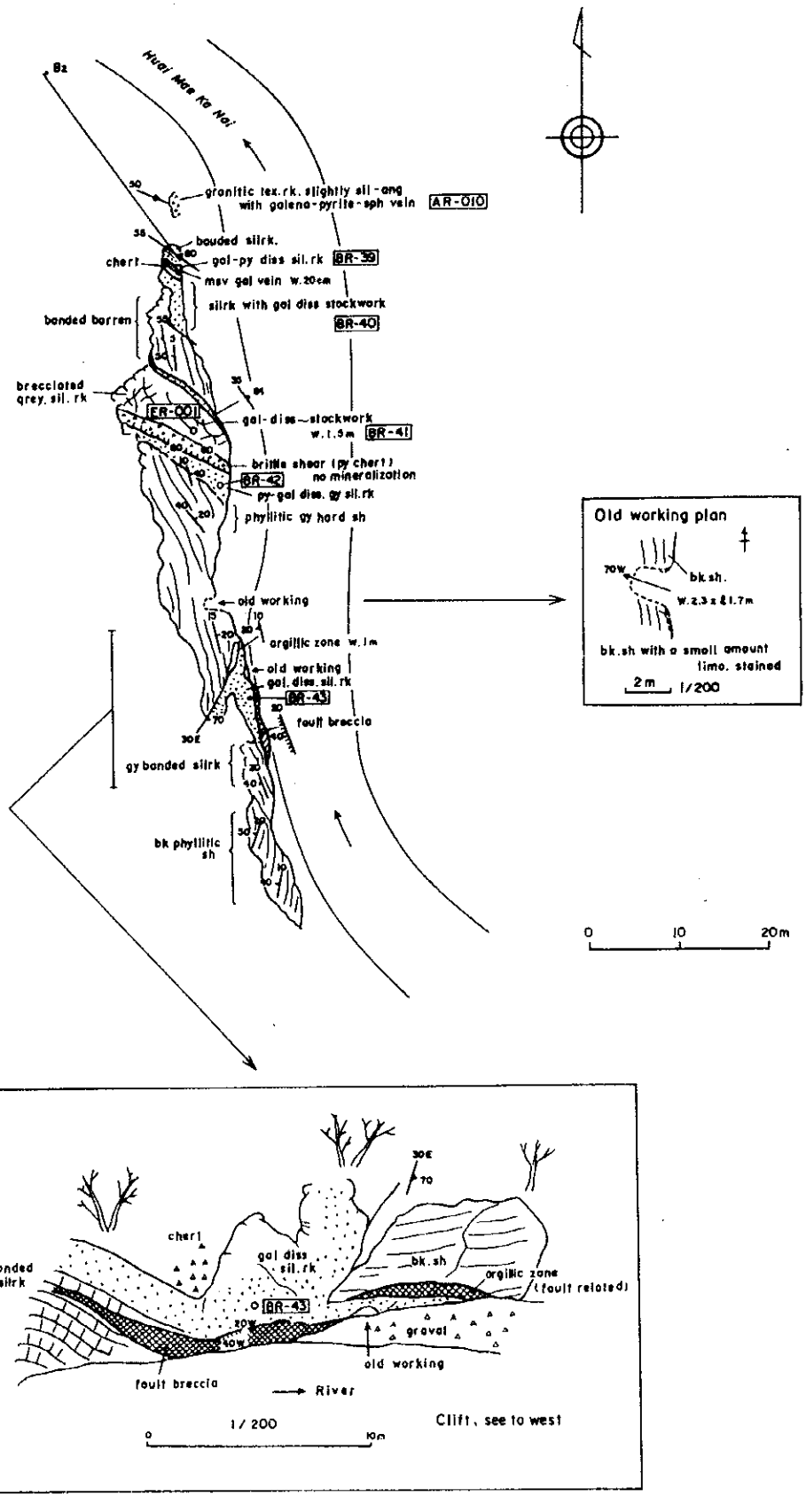

Fig.II-3-2 Sketch map of mineral occurrence along Nam Mae Kanai in the I-4 area

mineralized zone in the central part. The strike of the mineralized zone seems to be almost parallel to the direction of the fault breccia zone. It is concordant with the strike of the silicified shale of N 5 to 10° W. The dissemination - network vein zone is 1.5 m wide on the hanging wall side of the fault breccia zone and about 4 m wide on the foot wall side. No sulfide mineralization is observed in the fault breccia zone.

A more than 5 m wide galena - arsenopyrite dissemination exists on the hanging wall side of the fault breccia zone striking N 20° W and dipping 70° E parallel to a bedding plane of silicified shale in the mineralized zone on the south. The fault breccia zone is accompanied by dark gray clay and pyrite dissemination. According to the ore assay of the samples (BR043) taken from a part where galena - arsenopyrite strongly disseminated, Pb of 2.14 % was obtained.

There are two small survey pits near the mineralized zone on the south side. The one is a 1.7 m deep excavation site of weakly altered black shale in the direction of N 70° W. Alluvial gravels are accumulated on the pit bottom. As far as we can see the remains of the unsupported excavation, it is assumed that an excavation is carried out only up to the present heading. Only a slight dissemination of pyrite can be seen on black shale at the pit mouth and on the pit wall. This black shale has a lot of slightly irregular fractures. These fractures are filled with goethite. The other old survey pit is in the middle of the mineralized zone on the south side. Since this site is almost buried in the river gravels, it is not known how a tunnel is driven. Rocks near the pit mouth are silicified rocks strongly disseminated by galena - arsenopyrite.

3-5 Geochemical survey

3-5-1. Sampling

Samples were taken at intervals of 25 m on thetraverse lines in the geophysical survey in the I-4 area. Sampling points were arranged so that the entire area can be covered. Plate-10 shows the sampling points. The number of samples in the I-4 detailed survey area is 680.

3-5-2. Analysis of single component data

(1) Statistical processing

The common logarithm of each analysis value was used for analysis. As for an analysis value below the detection limit value in the statistical processing, a half value of that value was adopted. Also, as for an analysis value above the detection limit value, a limit value was adopted.

Statistics of each element are shown in Table II-3-1. Also, the frequency distribution of each element and the cumulative frequency curve are shown in Figs. II-3-3(1) to (3). The frequency distribution classification is 1/2 σ.

The correlation coefficients among elements are shown in Table II-3-2. Au, Ag, and Sn

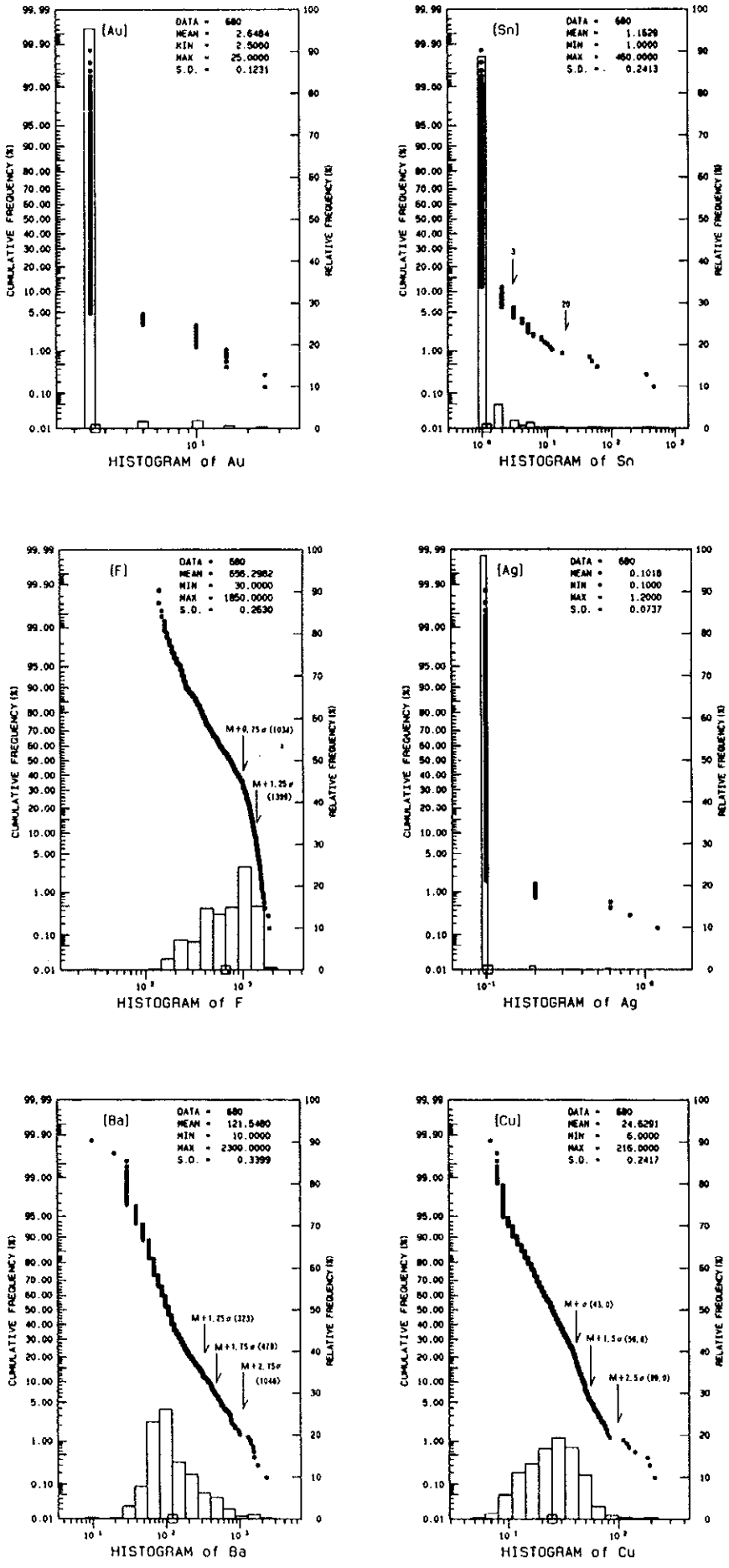

Fig.II-3-3 Relative frequency and cumulative frequency histogram of soil in the I-4 area(1)

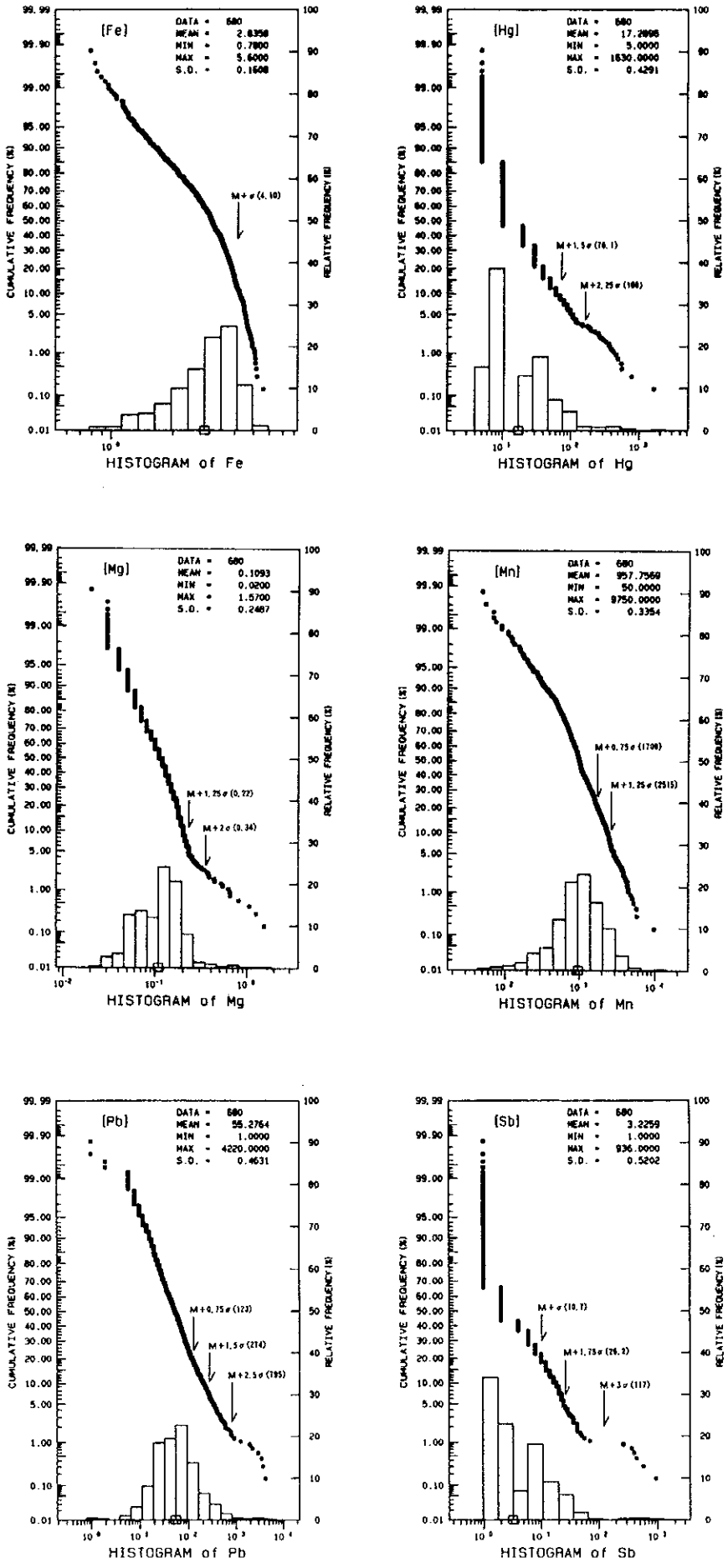

Fig.II-3-3 Relative frequency and cumulative frequency histogram of soil in the I-4 area(2)

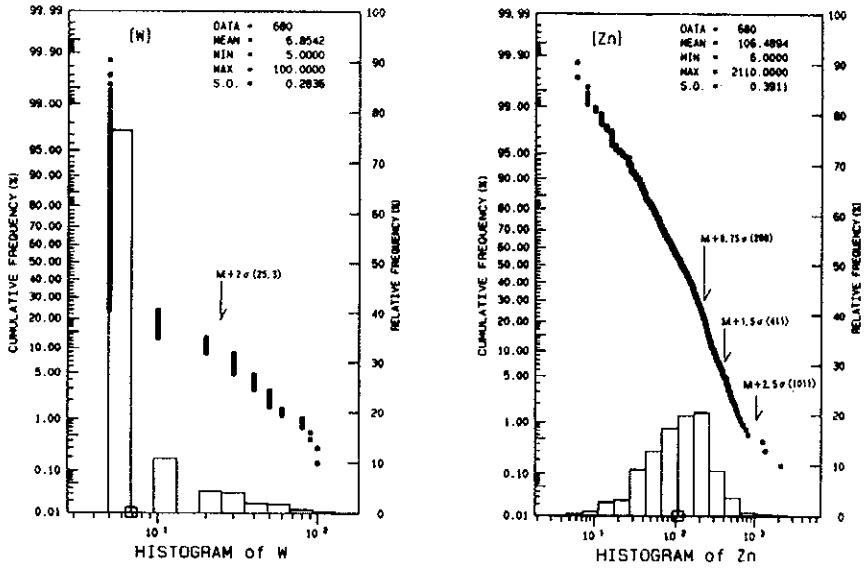

Fig.II-3-3 Relative frequency and cumulative frequency histogram of soil in the I-4 area(3)

Table II-3-1 Geochemical basic statistic quantities of soil samples in the I-4 area

Element	Unit	Lower Detection Limit	Maximum Value	Minimum Value	Average	Standard Diviation (log)
Au	ppb	5	25	<5	2.65	0.1231
Sn	ppm	2	460	<2	1.16	0.2413
F	ppm	20	1,850	30	656.30	0.2630
Ag	ppm	0.2	1.2	<0.2	0.102	0.0737
Ba	ppm	10	2,300	10	121.55	0.3399
Cu	ppm	1	216	6	24.63	0.2417
Fe	%	0.01	5.6	0.78	2.34	0.1608
Hg	ppb	10	1,630	<10	17.29	0.4219
Mg	%	0.01	1.57	0.02	0.11	0.2487
Mn	ppm	5	9,750	50	957.76	0.3354
Pb	ppm	2	4,220	<2	55.28	0.4631
Sb	ppm	2	936	<2	3.32	0.5202
W	ppm	10	100	<10	6.58	0.2836
Zn	ppm	2	2,110	6	106.49	0.3911

which are below the detection limit value of more than 98 % of the total analysis samples are excluded in finding the correlation coefficients.

Cu shows a strong positive correlation with Ba and has a weak positive correlation with Fe and Mn. Pb shows a very strong positive correlation with Zn and has a positive correlation with As, Ba, and Sb. Zn has a strong correlation with Fe, Pb, and As and also shows a positive correlation with Mg, Ba, As, F, and Fe. All things considered, these elements can be divided into two, Pb-Zn-As-Sb-Hg group and Cu-Pb-Ba-Mn group.

Table II-3-2 Geochemical correlation coefficients of soil samples in the I-4 area

	F	Ba	Cu	Fe	Hg	Mg	Mn	Pb	Sb	W	Zn	As
F	1.0000											
Ba	-0.1870	1.0000										
Cu	-0.3584	**0.5529**	1.0000									
Fe	0.4928	0.2827	0.2976	1.0000								
Hg	0.2839	-0.0284	-0.1448	0.1090	1.0000							
Mg	**0.5727**	0.2534	0.0895	**0.5672**	0.1436	1.0000						
Mn	-0.3202	**0.6171**	0.3594	0.1494	0.0054	0.1046	1.0000					
Pb	0.0455	**0.5833**	0.2829	0.3614	0.2223	0.1487	0.2491	1.0000				
Sb	0.2406	0.1194	-0.0267	0.3220	0.4515	0.1781	-0.0149	0.4904	1.0000			
W	0.3867	-0.1676	-0.2817	0.3374	0.3701	0.1166	-0.0676	0.1530	0.4651	1.0000		
Zn	0.3962	0.4431	0.2070	**0.5522**	0.3303	0.4278	0.1087	**0.8024**	**0.5217**	0.2725	1.0000	
As	0.1869	0.0851	-0.0001	0.2316	**0.5412**	0.0773	-0.0715	**0.5236**	**0.7680**	0.4465	**0.5099**	1.0000

(2) Distribution of geochemical anomaly

1) Determination of threshold

The threshold value is determined based on the average and standard deviation, taking the percentile of the frequency distribution and the break point of the cumulative frequency curve into consideration. Table II-3-3 shows threshold values of each element.

2) Distribution of geochemical anomaly

Figures II-3-4 to 7 show anomaly zones of each element.

[Zn] Anomalies of Zn are observed on both sides of the Ordovician limestone area and the Permian to Triassic sedimentary rock area. Anomalies in limestone are distributed at the northern end of traverse lines W, X, and Z and near the intersection point of these traverse lines and traverse line C. Although it is not certain, the distribution of these seems to con-

Table II-3-3 Division into geochemical anomaly levels of soil samples in the I-4 area

Element	Unit	Background	High anomaly1	High anomaly2	High anomaly3
Zn	ppm		M+0.75 σ 209	M+1.5 σ 411	M+2.25 σ 1,011
Pb	ppm		M+0.75 σ 123	M+1.5 σ 274	M+2.5 σ 795
Cu	ppm		M+ σ 43	M+1.5 σ 57	M+2.5 σ 99
Sb	ppm		M+0.75 σ 10.7	M+1.75 σ 26.2	M+3 σ 117
Au	ppb		5	10	
Ag	ppm		2		
Sn	ppm		3	20	
F	ppm		M+0.75 σ 1,034	M+1.75 σ 1,399	
Hg	ppb		M+1.25 σ 81	M+2.5 σ 182	
Mn	ppm		M+ σ 9,192		
Mg	%		M+1.5 σ 0.99	M+2.25 σ 2.19	
Fe	ppm		M+ σ 12.1		
Ba	ppm		M+0.75 σ 1,311	M+1.75 σ 3,772	

tinue in the north-south to north-northeast - south-southwest direction. This direction seems to be predominated by a foliated fracture system developed in limestone. Anomalies observed in the Permian to Triassic sedimentary rocks are distributed on the west side from the intersection point of traverse lines A and B and traverse line W, on the south side from the inter-

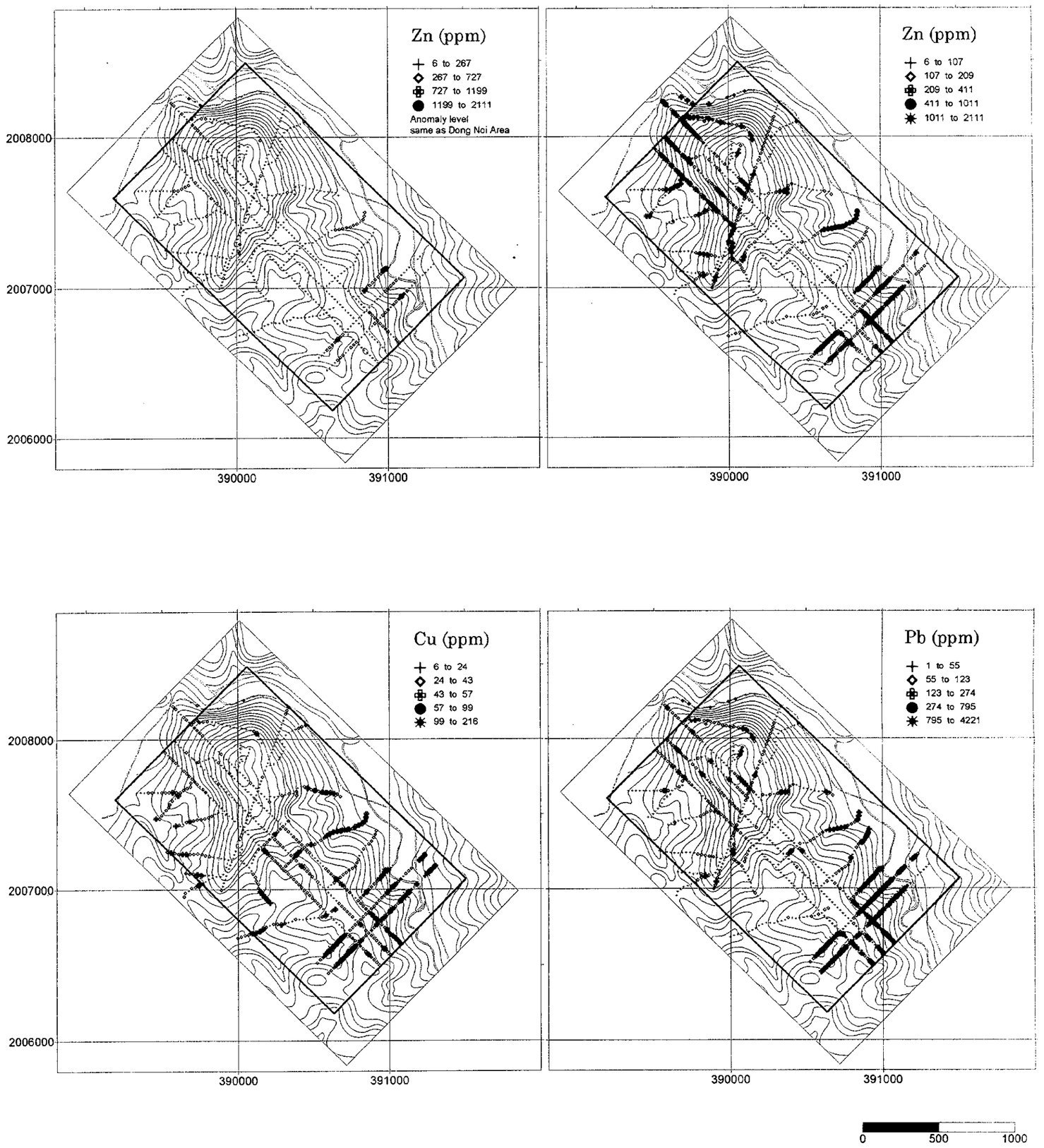

Fig.II-3-4 Geochemical map of Zn, Pb, Cu content in soil of the I-4 Area

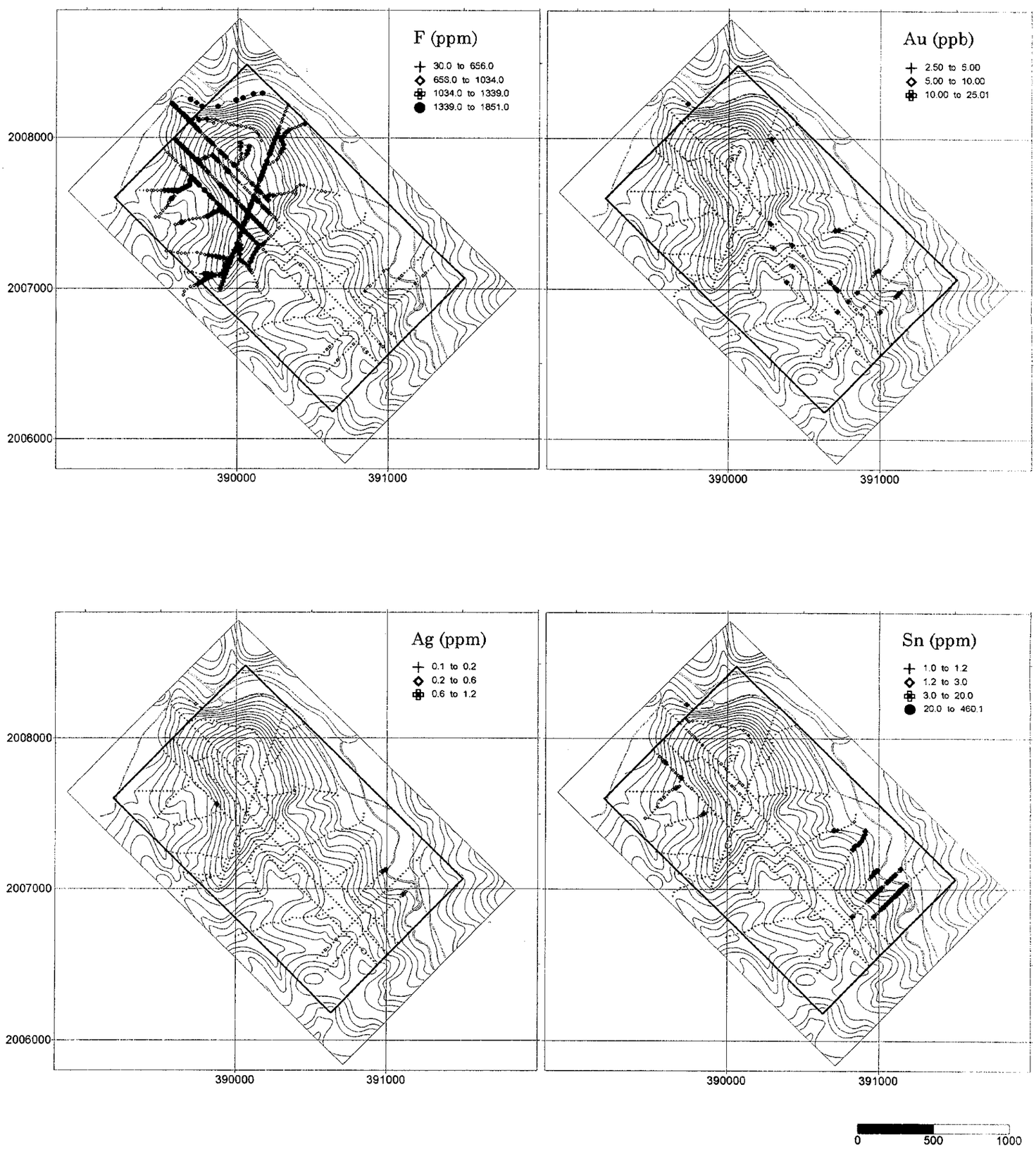

Fig.II-3-5 Geochemical map of F, Au, Ag, Sn content in soil of the I-4 Area

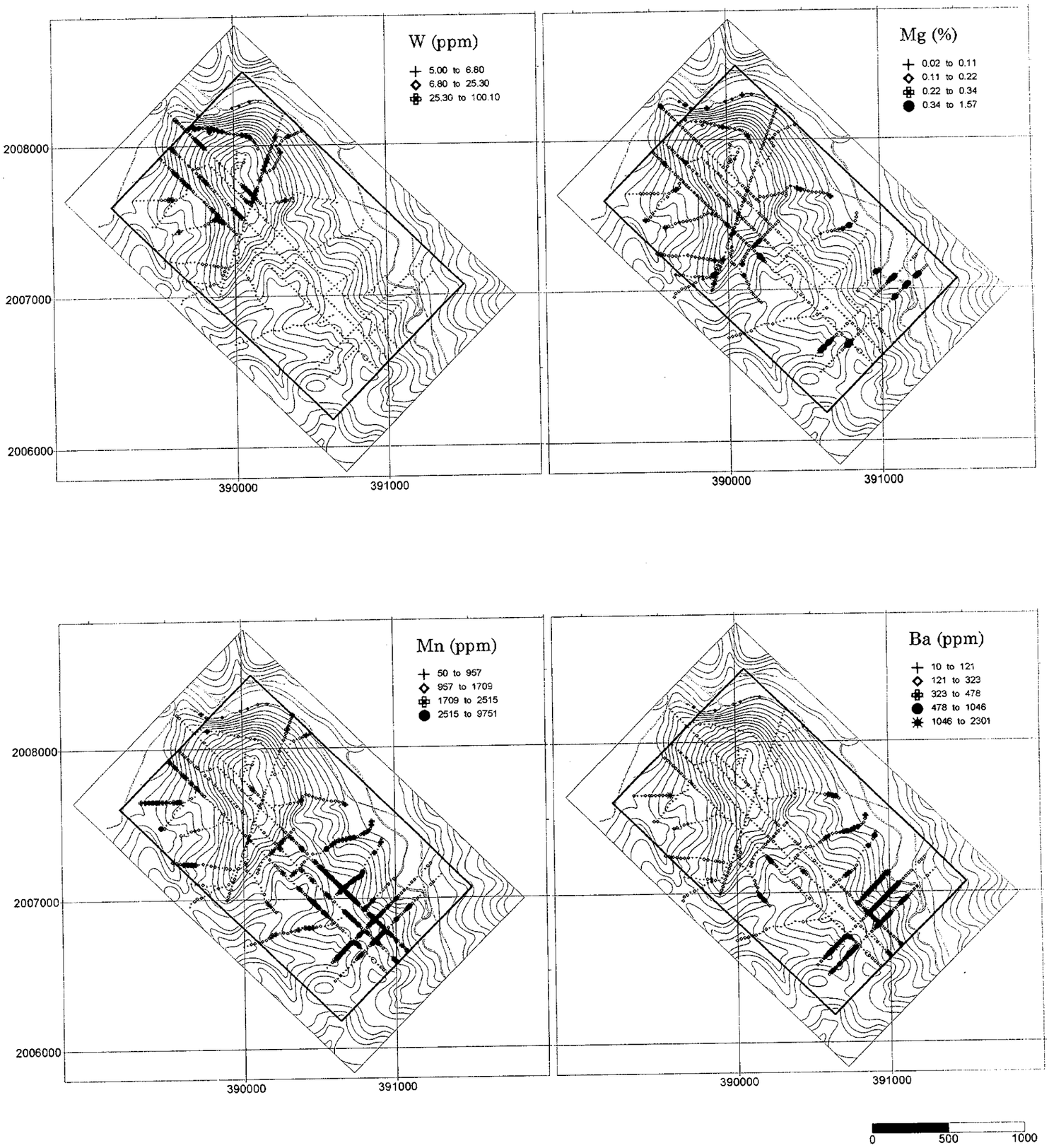

Fig.II-3-6 Geochemical map of W, Mg, Mn, Ba content in soil of the I-4 Area

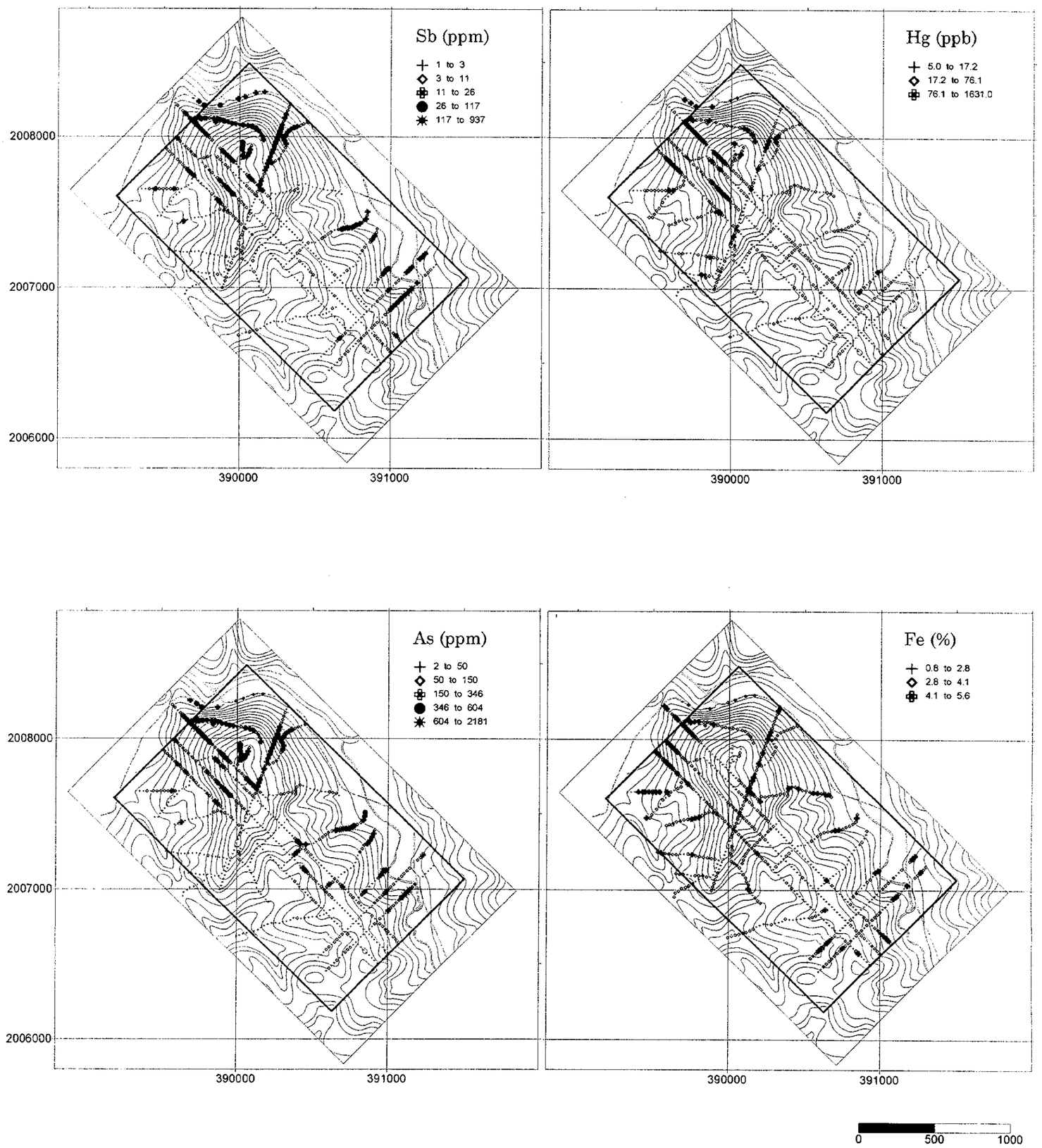

Fig.II-3-7 Geochemical map of Sb, Hg, As, Fe content in soil of the I-4 Area

section point of traverse line Y and traverse line A, at the point of 600 m to 700 m of traverse lines A and B and on its northwest side. Among these anomalies, it is thought that the latter corresponds to floats of galena - quartz vein in a mineralized zone at 800 m point of traverse line B and on its northwest extension and the former corresponds to floats of barite with galena dissemination. Anomalies are also observed in shale along the marsh in the center of the area. It is thought that this anomaly is distributed along a fault.

[Pb] The distribution of Pb anomalies is similar to that of Zn anomalies. The values in the limestone area are low but are high in the sedimentary rock area, particularly, near the ore occurrence along traverse line B. Like Zn, the anomalies is also observed in the central part of the area.

[Cu] Cu shows the same distribution as Pb and Zn near traverse lines A and B and in a marsh in the central part of the area. In other parts, Cu anomalies overlap on shale. It is thought that a part of it represents an existence of shale having a initially high Cu value.

[F] The F anomalies are distributed in the Ordovician limestone area. This distribution is harmonious with that of Zn and Cd anomalies. In many cases, samples having an average Zn value are classified as anomaly values. Judging from an existence of a fluorite deposit in limestone on the north side of this area, it may be an extension of this ore showing. The anomalies reach out in the same direction as Zn from almost north and south to slightly east.

[Au] Samples lower than the detection limit value account for 90 %. The content of Au is maximum 25 ppb, which is far from an anomaly value. Samples of a high Au concentration are scattered in the upper part of the ore showing in the eastern part of the area.

[Ag] There are no samples having an anomaly value.

[Sn] The Sn anomalies overlaps that of the Zn and Pb anomalies in the eastern part of the area. According to the ore assay results in an outcrop of the ore showing, a value of Sn > 1,000 ppm was obtained. The Sn content seems to be high in the anomaly area on the east side.

[W] The W anomalies exist in the limestone area and appear accompanied by fractures.

[Mg] The high Mg anomalies, which concentrate in the eastern part of the area, are found in small numbers in the limestone area.

[Mn] The Mn anomalies concentrates in the eastern part of the area. Although in some parts they overlap the Zn and Pb anomalies, the Mn anomalies are found at a higher place in altitude than the Zn and Pb anomalies.

[Ba] The Ba anomalies appear only in the eastern part of the area and its distribution overlaps that of the Pb and Zn anomalies.

[Sb] The Pb anomalies are high on the ore showing in the eastern part of the area and their distribution is similar to that of the Sn anomalies. The distribution of low anomaly is also observed in the limestone area and this distribution form is similar to that of the W anomalies.

[Hg] This does not show such high values as to be called anomaly values. Samples of high concentration are distributed in the outcrop of galena, in the eastern part of traverse line E, in the low land area on the northwest side of the area.

[As] The As anomalies is similar to that of the Sb anomalies.

[Fe] The Fe anomalies are observed also in anomaly areas of other elements in the eastern part of the area, but the northern end of the area shows higher values as anomaly values.

3-5-3 Principal components Analysis

Analysis of principal components was made on the correlation matrix found from a logarithmic value of soil analysis values. The results are shown in Table II-3-4.

The eigenvalue shows 1 or more up to the third principal components, the contribution rate shows 10 or more up to the third principal components. The cumulative contribution rate is 69 % up to the third principal components. It is judged significant up to the third principal components. The principal component score is shown in Fig. II-3-8.

[Z-1] The factor loading amount of Zn, Pb, Sb, As, Fe, W, and Mg is large and F and Ba show the factor loading amount to some extent. Z-1 is considered to be a factor that reflects an existence of mineral showings of these elements. A high-score zone is roughly distributed in four places. One is distributed beneath an intercalation of shale and sandstone at the north end of the area. Particularly, it is continuously observed in the north and south direction at the foot of the mountain on the west side and on the east side of the mountaintop. The high

Table II-3-4 Results of principal analysis of soil samples in the I-4 area

Principal component	Eigen-value	Contribu-tion rate %	Cumula-tive rate %	Factor loading	Z-01	Z-02	Z-03
Z-01	4.0950	34.1250	34.1250	Zn	**0.8683**	0.1365	0.0542
Z-02	2.6297	21.9142	56.0392	Pb	**0.7462**	0.3583	-0.2584
Z-03	1.6325	13.6042	69.6434	Sb	**0.7458**	-0.2224	-0.3670
Z-04	0.8566	7.1383	76.7817	As	**0.7182**	-0.2380	-0.4949
Z-05	0.7121	5.9346	82.7163	Fe	**0.6797**	0.0973	**0.5081**
Z-06	0.6362	5.3013	88.0176	Hg	**0.5209**	-0.3470	-0.3051
Z-07	0.4548	3.7898	91.8073	Ba	0.4202	**0.7955**	0.0113
Z-08	0.2848	2.3737	94.1810	Cu	0.1691	**0.7628**	0.0235
Z-09	0.2210	1.8415	96.0225	Mn	0.1647	**0.6846**	-0.0508
Z-10	0.2040	1.7002	97.7227	W	**0.5026**	-0.5039	-0.0941
Z-11	0.1712	1.4268	99.1495	Mg	**0.5173**	0.0143	**0.7003**
Z-12	0.1021	0.8505	100.0000	F	0.4759	-0.5561	**0.5740**

score zones show a wide range. On the east half of the area, the high score zone is divided into three parts showing a narrow range. A high-score zone around the 700 m point along traverse line B continues in the north and west direction via the 700 m point along traverse line A. On the starting point side along traverse lines A and B, an anomaly area having a center on the side of traverse line A is formed. Another high score zone is observed along a

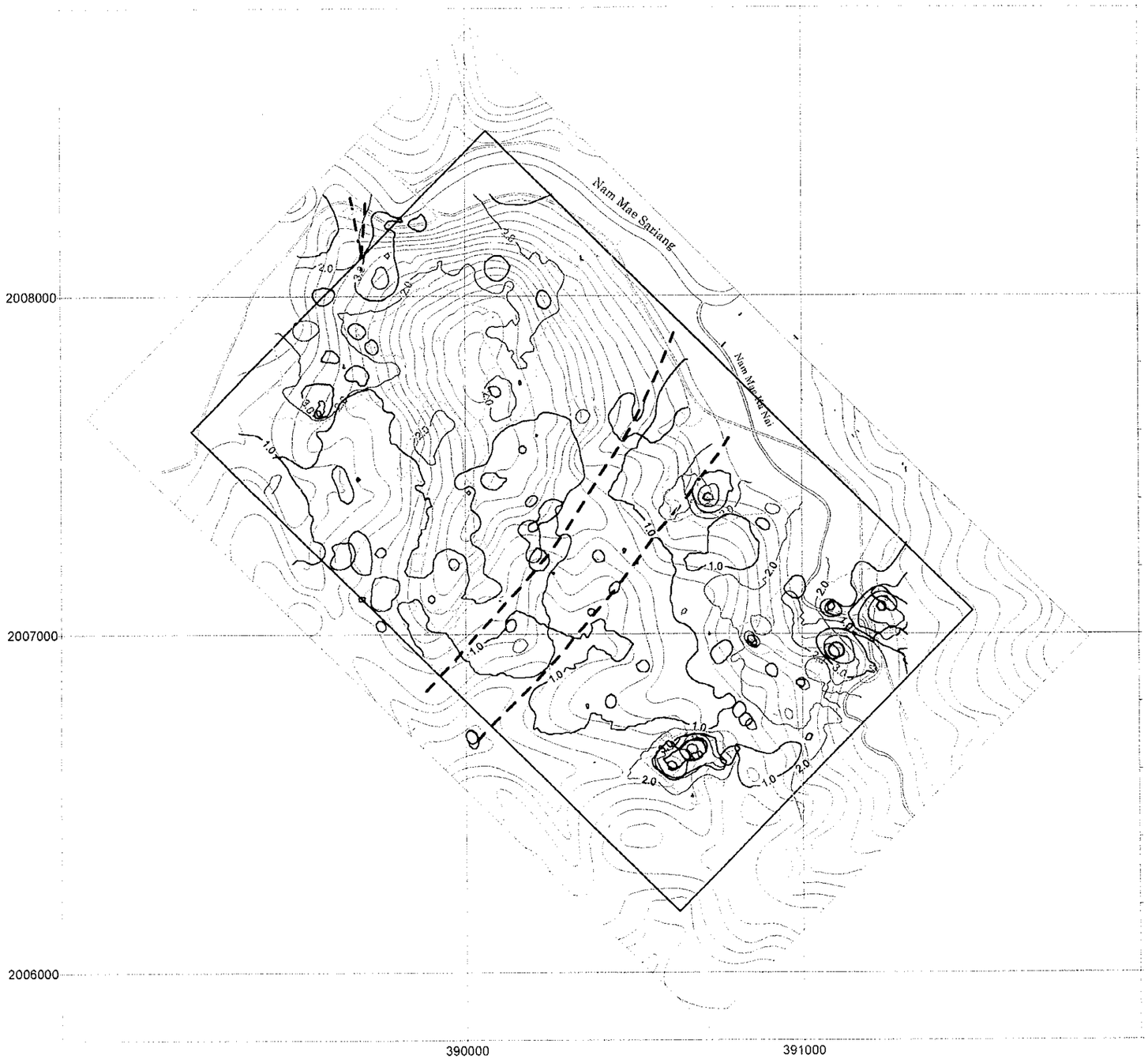

Facter loading

	Z-01	Z-02	Z-03
Zn	0.8683	0.1365	0.0542
Pb	0.7462	0.3583	-0.2584
Sb	0.7458	-0.2224	-0.3670
As	0.7182	-0.2380	-0.4949
Fe	0.6797	0.0973	0.5081
Hg	0.5209	-0.3470	-0.3051
Ba	0.4202	0.7955	0.0113
Cu	0.1691	0.7628	0.0235
Mn	0.1647	0.6846	-0.0508
W	0.5026	-0.5039	-0.0941
Mg	0.5173	0.0143	0.7003
F	0.4759	-0.5561	0.5740

Z-1
score 5
score 4
score 3
score 2
score 1

Z-2
score 4
score 3
score 2
score 1

Z3
Score 4
Score 3
Score 2
Score 1

fault

0m 500m 1000m

Fig. II-3-8 Principal analysis score map of the I-4 area

marsh in the center of the area. This anomaly area is accompanied by a NE-SW fault. However, an anomaly of neither this principal component nor other principal components is observed in other part of this fault.

[Z-2] As for the second principal component, the factor loading amount of Cu, Ba and Mn is large and Z-2 is considered to be a factor which represents the mineralization of these elements. A high-score zone having three points or more overlaps a high-score zone of the first principal component near the 100 m point along traverse line A and shows a narrow distribution range. It is also distributed near the 700 m point along traverse line B, at the bending point of Nam Mae Ka Nai on the northwest side of that point, etc. The distribution of scores having three points or less roughly matches that of shale so that there is probably suggested that this indicate the initial concentration of Cu and Mn in shale.

[Z-3] This is the principal component that has a large factor loading amount of Fe, Mg, and F. It seems to be distributed on the periphery of a high-score area of the first principal component. This is presumably indicating a halo of mineralization shown by the first principal component.

3-6 Geophysical Survey

3-6-1 Measurement of rock properties(1) Measurement result The measurement result of rocks and ore samples were shown in Table Ⅱ-3-5, Fig. Ⅱ-3-9.

Also, the rock acquisition location of the I-4 area was shown in Fig. Ⅱ-3-10.

In the I-4 area, it acquired 18 samples. The apparent resistivity shows from 88Ω·m to 19440 Ω·m value and the chargeability shows a maximum of 58 mV·sec/V ,very high .

In this area, shales(BR040,BR043,BR044) which contained galena indicate very high chargeability above 50mV·sec/V. These samples were gathered around the ore bearing place which is located in the station 800 neighborhood of line B. As for BR045 which was gathered in the place which is near the same ore bearing place. The chargeability is low but it thinks that this is because it doesn't contain mineral.

The other sample shows the chargeability which is low for the most part regardless of the kind of rock. But, FR014 of chert is 12.6 mV·sec/V , rather high value.

Table Ⅱ-3-5 Resistivity and chargeability of rock samples in the I-4 area

Sample name	Rock name	Resis. (Ω·m)	Charge. (mV·sec/V)
AR040	Muddy limestone	6494	1.2
BR040	Silicified shale with galena-arsenopyrite diss.	637	58.8
BR043	Silicified shale with galena diss.	1367	58.2
BR044	Phyllitic shale with sulphide	582	52.9
BR045	Black shale	80.2	1.4
BR046	Bedded limestone	4340	3.8
BR047	Limestone with calcite veinlets	6319	4.6
BR048	Limestone with calcite veinlets	4356	4.4
BR049	Chert	14920	3.2
CR020	Fossiliferous limestone	4145	3.0
CR031	Calcareous shale	2090	8.2
CR032	Alternation of limestone and shale	113	1.1
DR027	Massive limestone	3689	3.1
DR028	Foliated limestone	4292	7.0
DR032	Calcareous sandstone	500	5.9
DR033	Phyllitic shale	88.8	0.2
FR009	Marble	19440	0.3
FR014	Bedded chert	4234	12.6

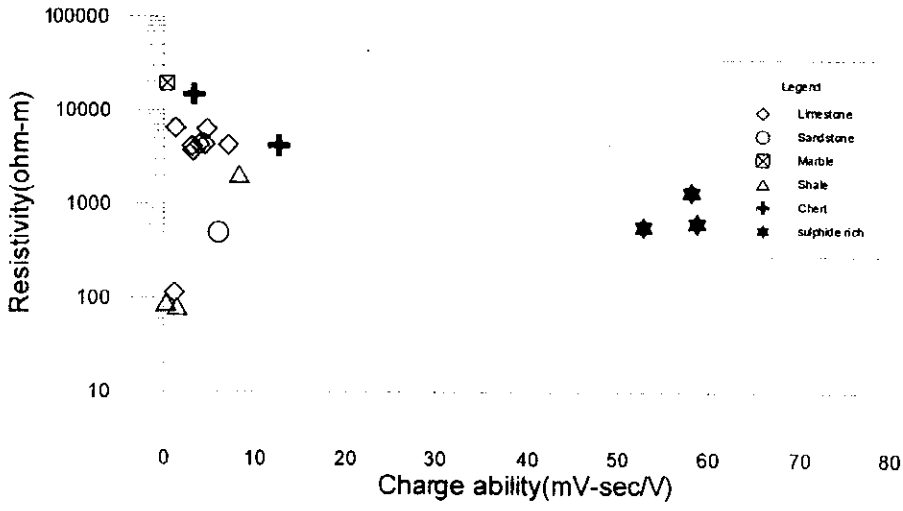

Fig.II-3-9 Resistivity and Chargeability of rock sample in the I-4 area

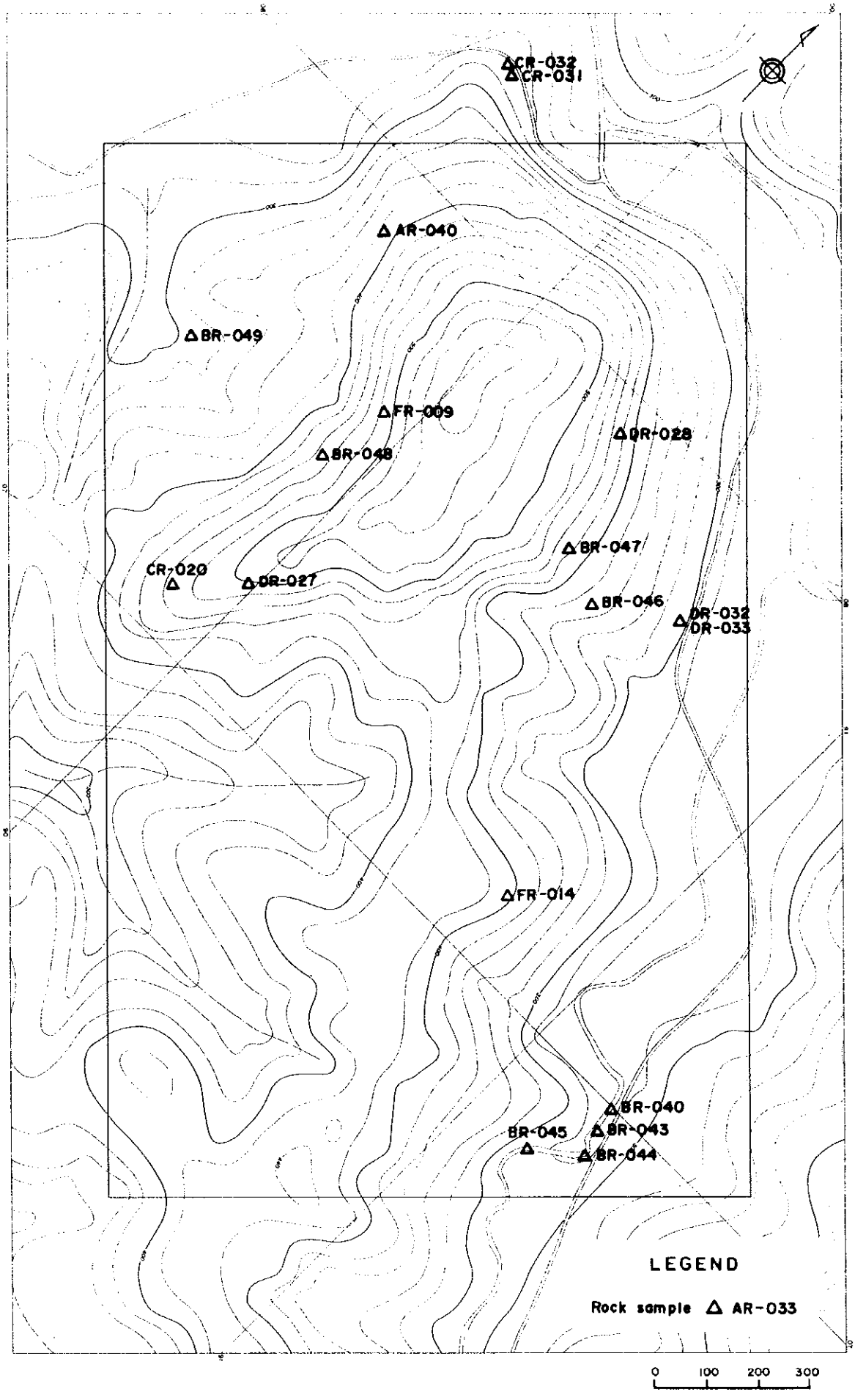

Fig.II-3-10 Locality of rock samples for laboratory test of the I-4 area

3-6-2 Measurement result

(1) Line setting

In this area, it set total line length of 9.8 km in amount which 1 X 1.3 Km length with the direction of N20° E ,2 X 1.0Km length with the direction of N45° E and 4(1 X 0.9Km , 1 X 1.6Km ,2 X 2.0Km)with the direction of N45° W.

Line locations are shown in Fig. II -3-11.

(2) Measurement result

1) Line A (Fig. II -3-12)

The apparent resistivity shows from 32Ω·m to 294 Ω·m value. The distribution of the apparent resistivity of more than 200 Ω·m is seen in the both edge of the line but the other part shows the value which is low for the most part. Especially, the apparent resistivity of less than 100 Ω·m is distributed between station 400 and 700 from the shallowness. Also, the distribution of the apparent resistivity of less than 100 Ω·m is seen to the shallowness between station 200 and 300, too.

The chargeability is the value from 10 to 57mV·sec/V and shows (above 20mV·sec/V) high chargeability approximately over all lines. The distribution of the chargeability of convex type is seen by the part the vertex of which was the bottom of about station 300. Also, it is high chargeability between station 400 and 900, too, but the distribution range is wide and it is difficult to grasp the vertex of the IP anomaly.

2) Line B (Fig. II -3-13)

The tendency with apparent resistivity and chargeability is similar to line A.

The apparent resistivity shows from 26Ω·m to 305 Ω·m value. The distribution of the apparent resistivity of more than 200 Ω·m is seen in southwestern part of the line, but the other part shows the value of the lowering for the most part and the apparent resistivity of less than 100 Ω·m is widely distributed between station 400 and 900. Also, the apparent resistivity of less than 100 Ω·m is seen under station 300, too.

The chargeability shows the value from 6 to 58mV·sec/V. Except for the shallowness between station 100 and 600, high chargeability is approximately shown in all lines (Above 20mV·sec/V). The distribution of the chargeability of convex type is seen by the part the vertex of which was the bottom of station 200. Also, it is high chargeability between station 400 and 900, too, but the distribution range is wide and it is difficult to grasp IP anomaly vertex.

3) Line C (Fig. II -3-14)

The apparent resistively shows from 160Ω·m and 4896 Ω·m value. It makes 300 Ω·m contour from the shallowness of station 1100 to the depth of station 800 a boundary , the side of its south shows the amount apparent resistivity of more than 1000 Ω·m and the northern side shows the apparent resistivity of about 200 Ω·m. This thing shows that the non- continuation part exists from the shallowness of station 1100 to the depth of station 800.

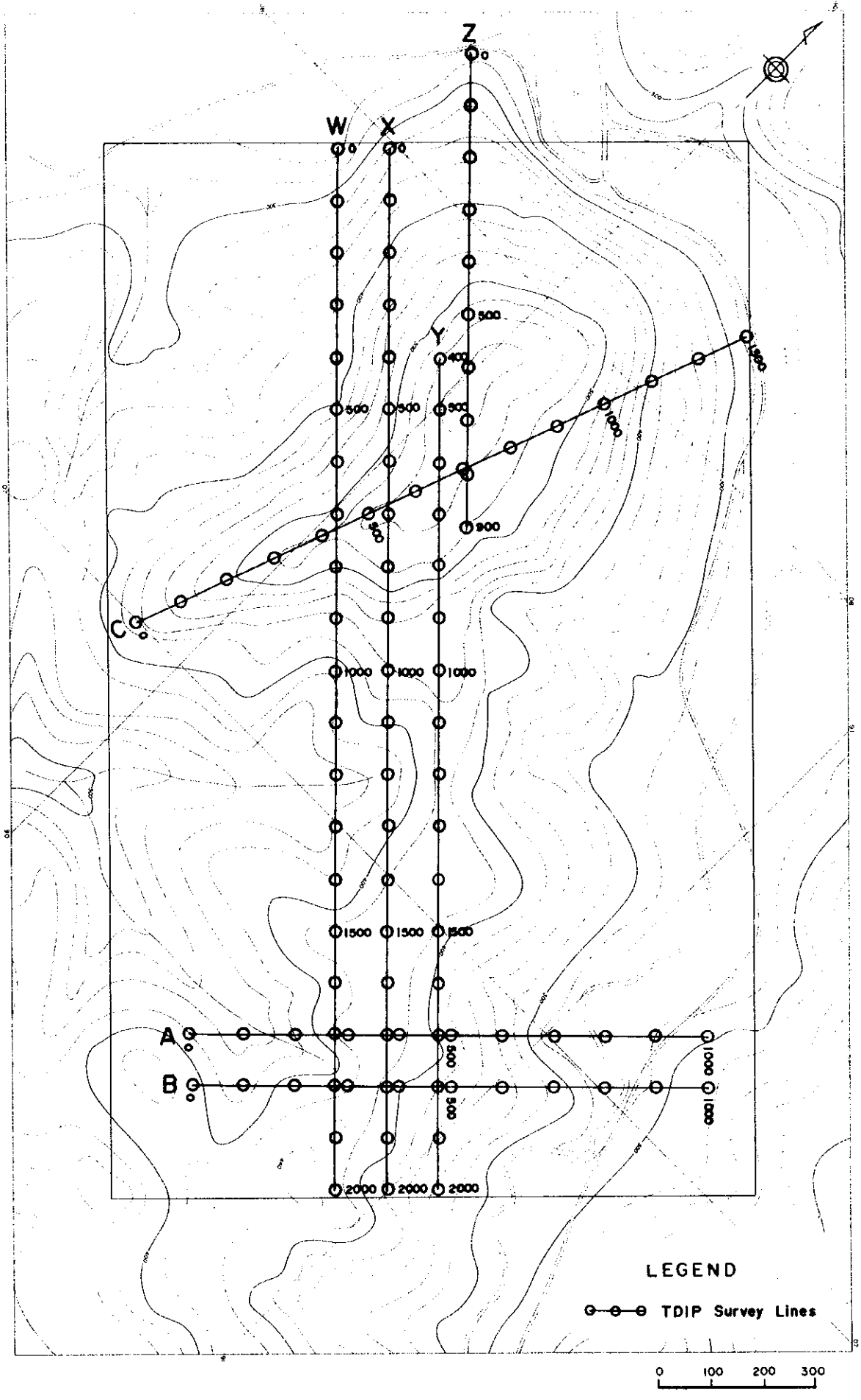

Fig.II-3-11 Location of survey line in the I-4 area

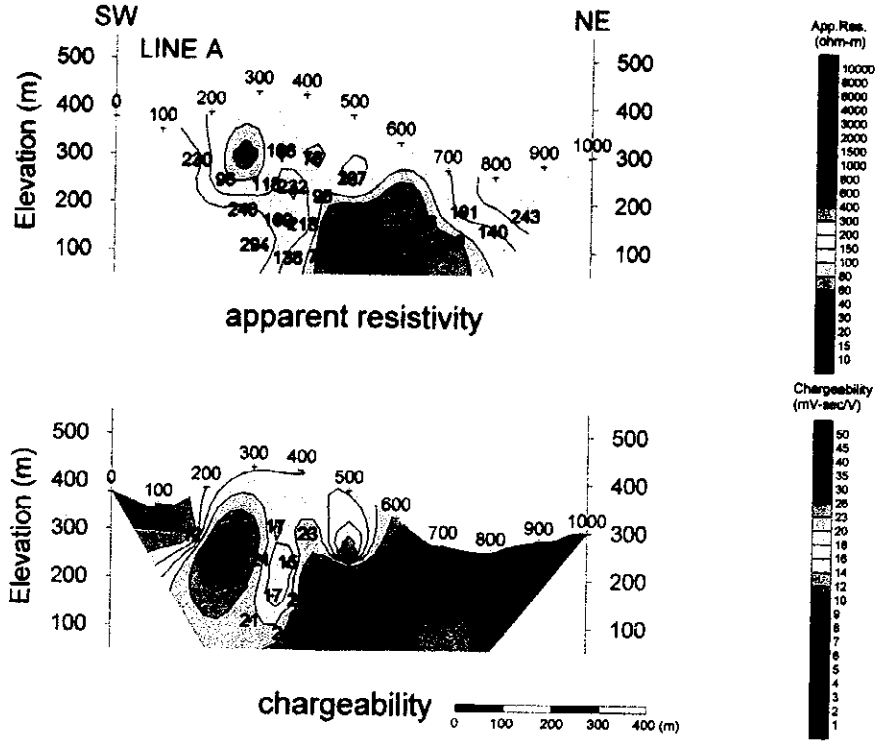

Fig.II-3-12 Pseudosection of apparent resistivity and chargeability of the I-4 area(A)

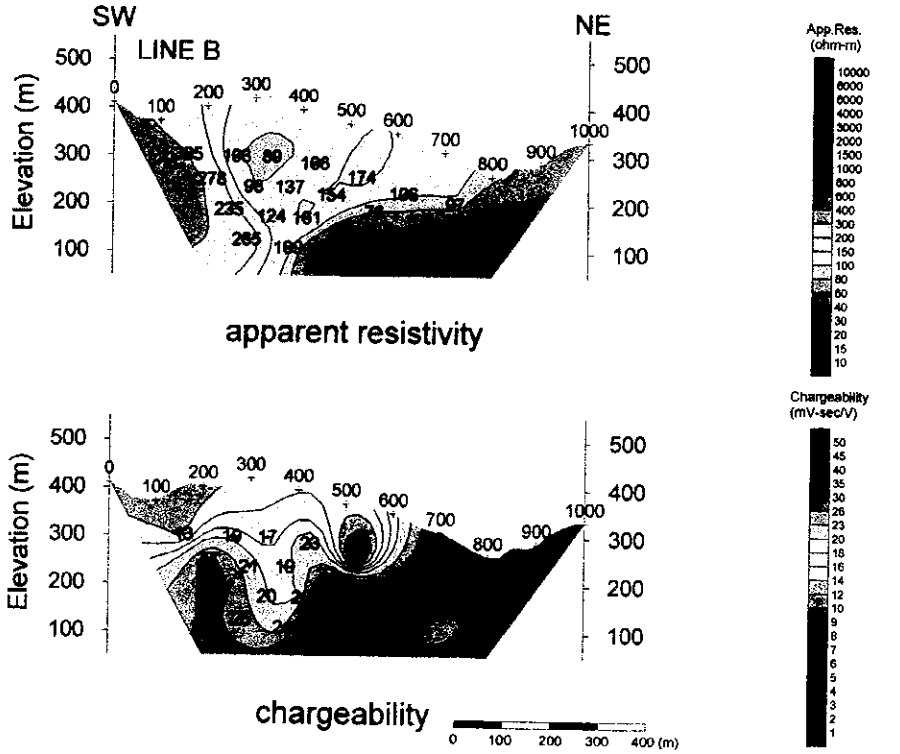

Fig.II-3-13 Pseudosection of apparent resistivity and chargeability of the I-4 area(B)

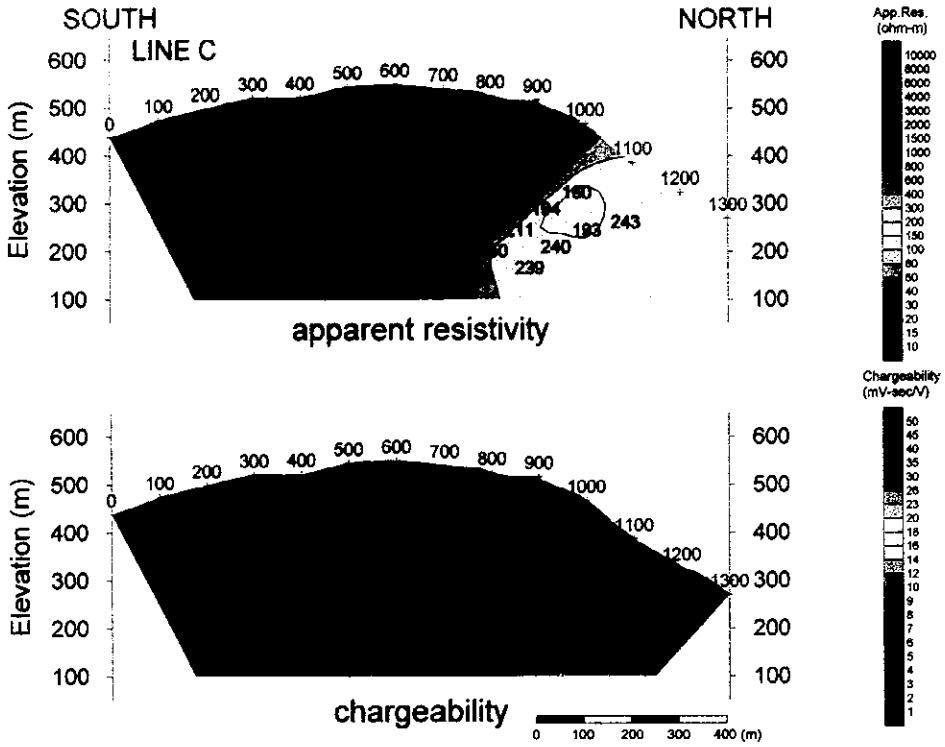

Fig.II-3-14 Pseudosection of apparent resistivity and chargeability of the I-4 area(C)

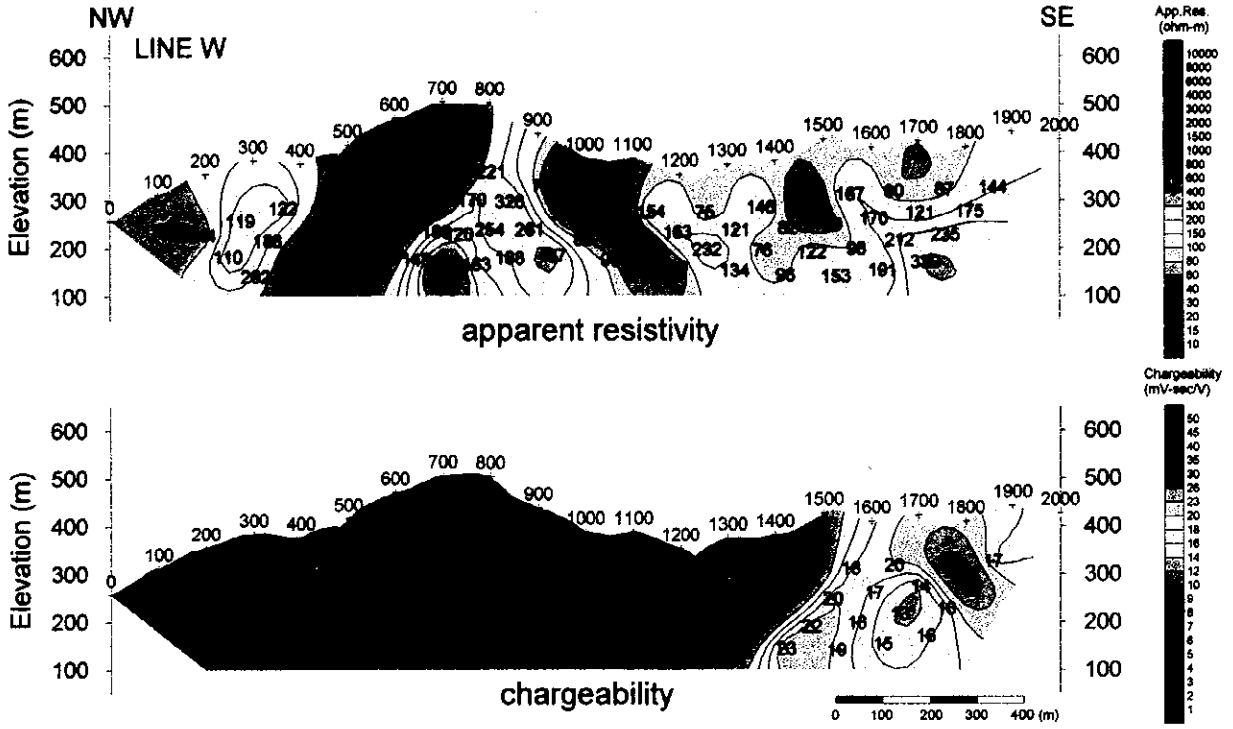

Fig.II-3-15 Pseudosection of apparent resistivity and chargeability of the I-4 area(W)

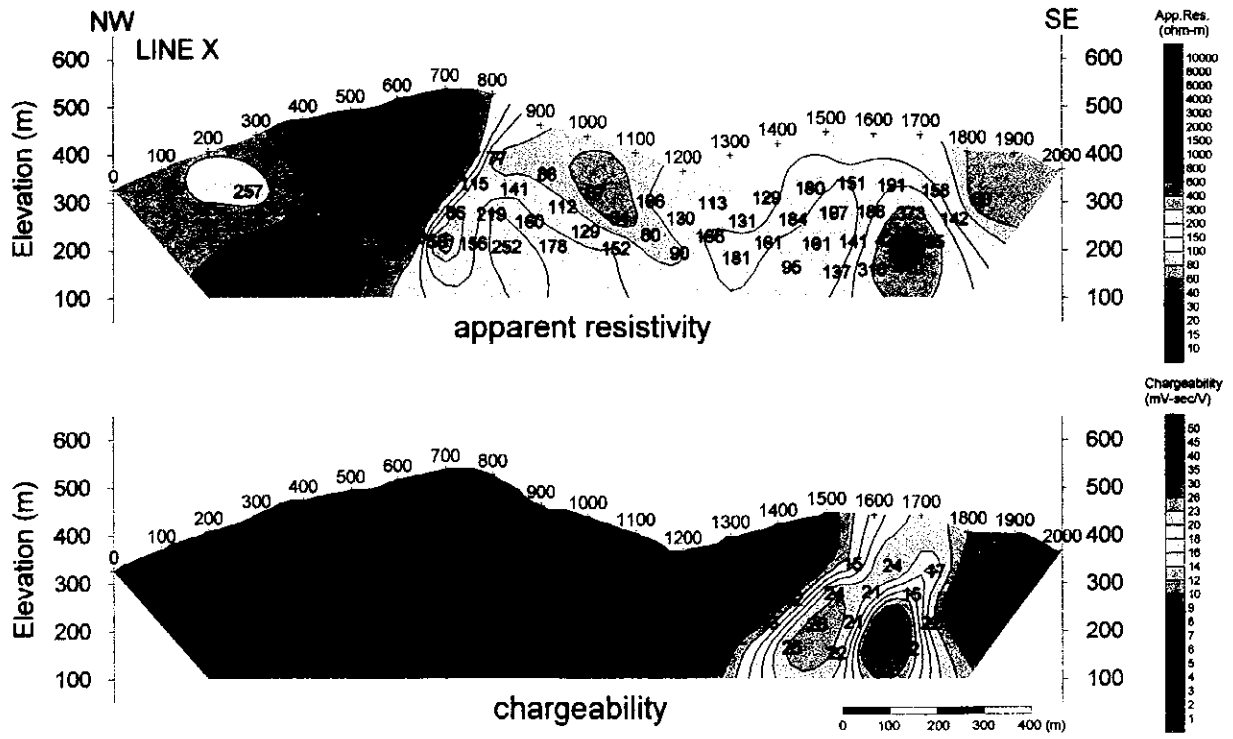

Fig.II-3-16 Pseudosection of apparent resistivity and chargeability of the I-4 area(X)

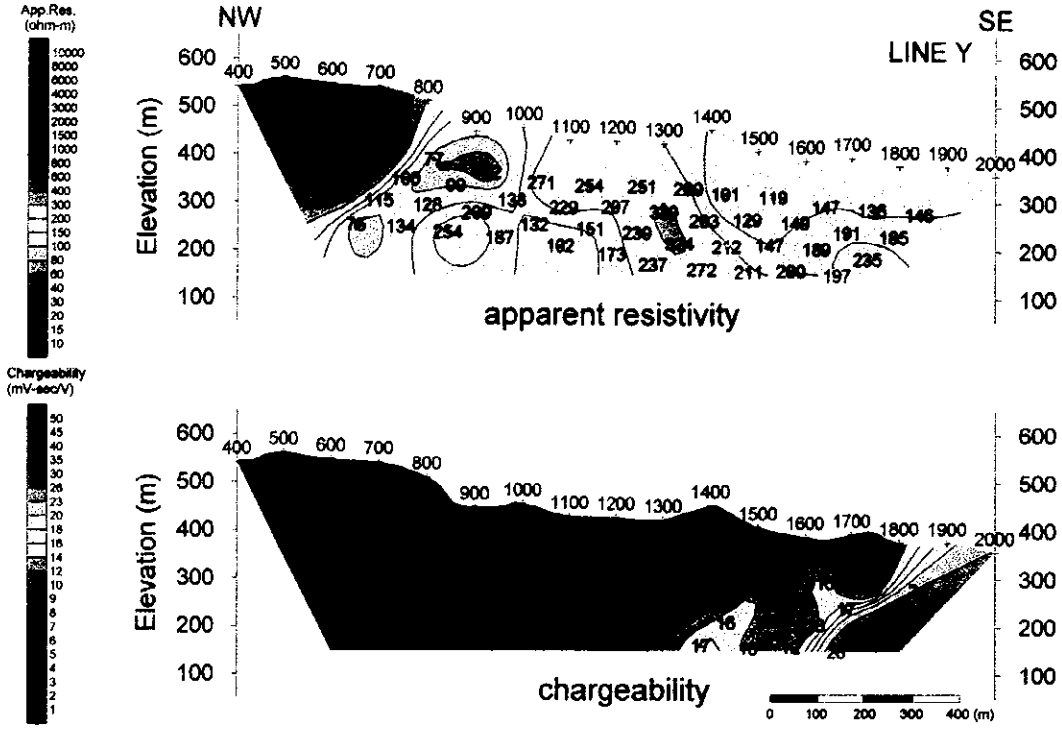

Fig.II-3-17 Pseudosection of apparent resistivity and chargeability of the I-4 area(Y)

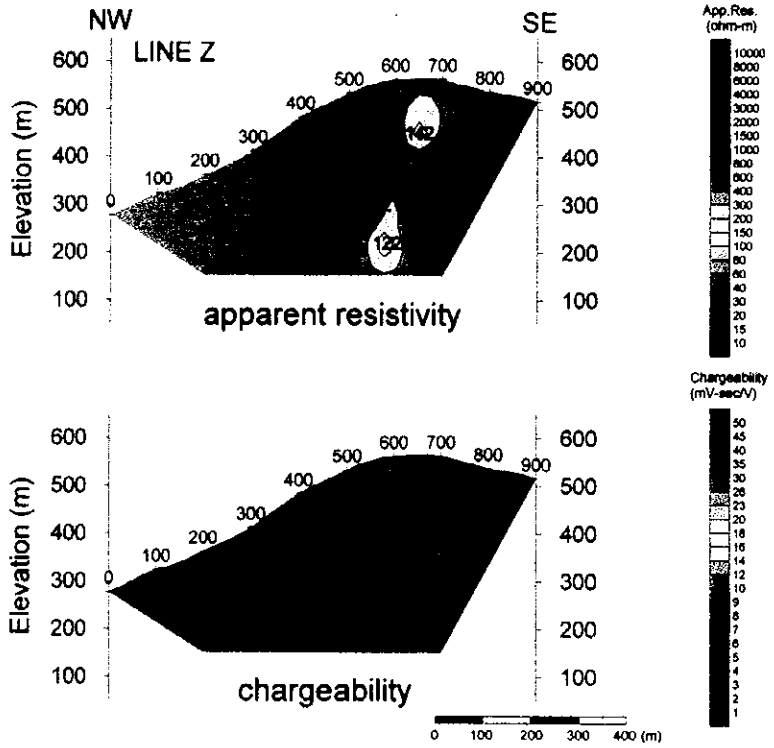

Fig.II-3-18 Pseudosection of apparent resistivity and chargeability of the I-4 area(Z)

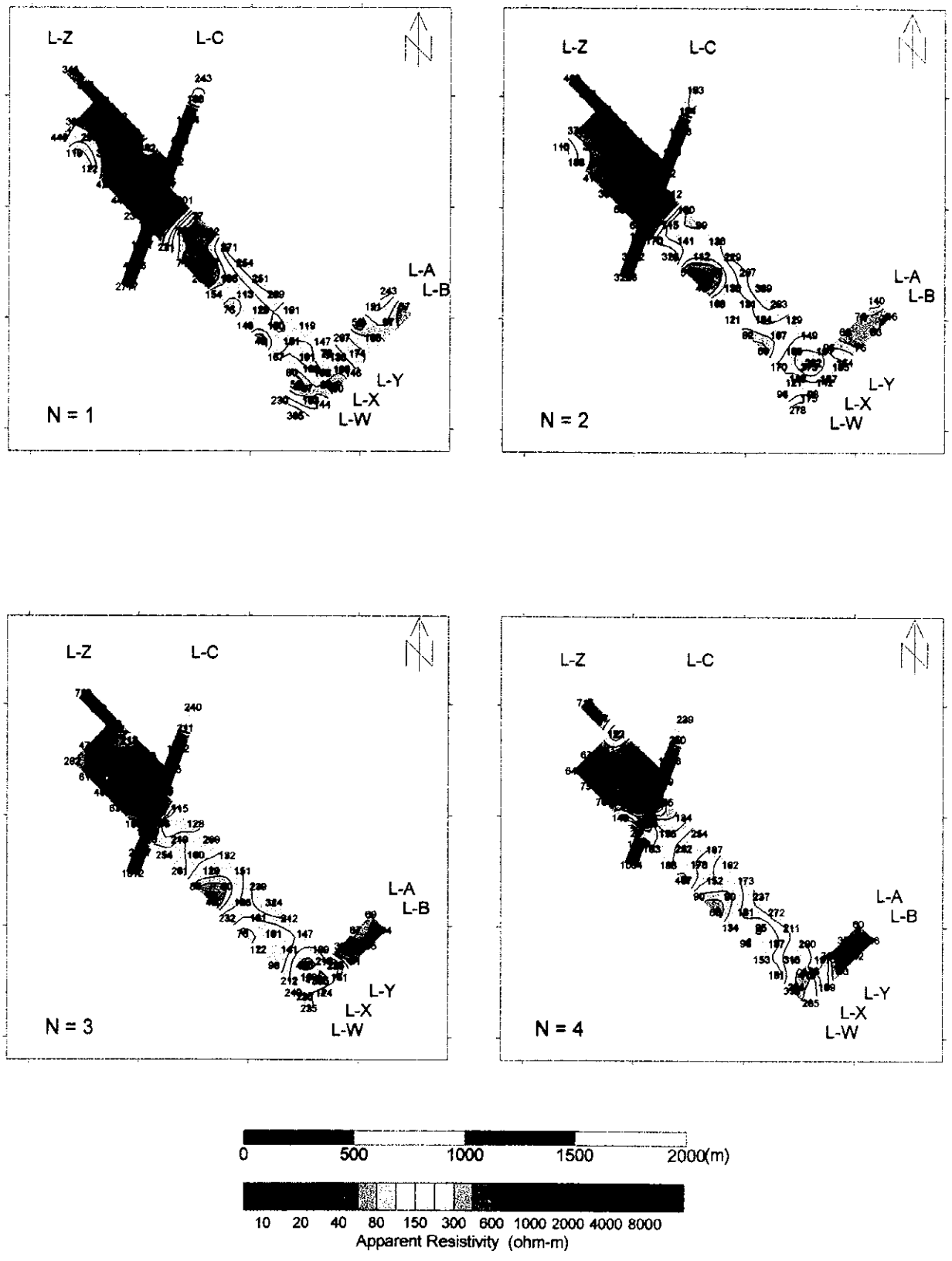

Fig II-3-19 Plan map of apparent resistivity of the I - 4 area

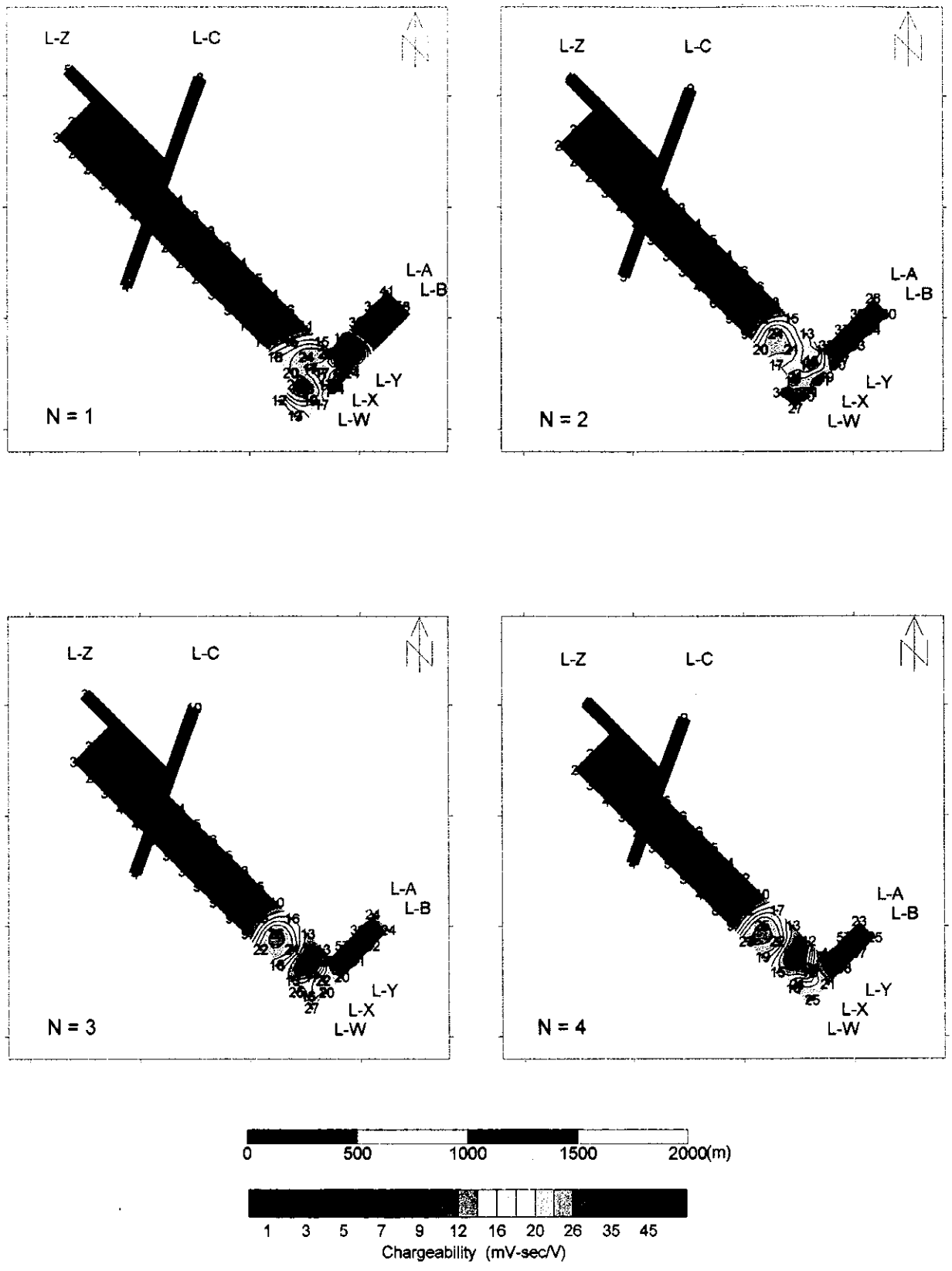

Fig.II-3-20 Plan map of chargeability of the I - 4 area

The chargeability shows the value from 3 to 10mV·sec/V and is low severely over all line. Also, it doesn't see IP anomaly area, too.

4) Line W (Fig. II-3-15)

The apparent resistivity shows from 25Ω·m to 750 Ω·m value. The distribution of the apparent resistivity of more than 200 Ω·m is seen to the depth of the northwest end of the line, between station 400 and 900 and between station 1600 and 1800. The part which shows the apparent resistivity of less than 100 Ω·m is seen in the depth of station 700, the shallowness between station 900 and 1100, between station 1200 and 1800 and under about station 1400 (continuing from the shallowness). The low apparent resistivity part which distributed over between station 900 and 1100 especially. The northwestern side shows the apparent resistivity of more than 200 Ω·m from station 900 - 1100 , and the southeastern side shows about 100 Ω·m. And this trend means that station 900 - 1100 form the boundary of the apparent resistivity between the northwest and southeast clearly.

Also, the part which shows from 100Ω·m to 200 Ω·m under about station 300, too, rather differ from the neighbor part in the value of the apparent resistivity .

The chargeability shows the value from 2 to 30mV·sec/V. In the border of the station 1600 shallowness to the station 1400 depth, the northwestern side becomes low chargeability and the southeastern side becomes high chargeability. In this high chargeability part, the distribution of the chargeability of convex type at the vertex of which is the neighborhood of station 1700 can be seen.

5) Line X (Fig. II-3-16)

The whole tendency is similar to line W. The apparent resistivity shows from 53Ω·m to 1826 Ω·m value. The distribution of the apparent resistivity of more than 200 Ω·m is seen by the northwestern side from station 800, the depth of station 900 and between station 1600 and 1800. The part which shows the apparent resistivity of less than 100 Ω·m is mainly distributed over between station 900 and 1200, and it makes this part a boundary and the tendency of apparent resistivity is different from the northwestern side to the southeastern side at this part.

The chargeability shows the value from 1 to 34mV·sec/V. In the border from the shallowness of station 1600 to the depth of station 1400, the northwestern side becomes low chargeability and the southeastern side becomes high chargeability. In this high chargeability part, the distribution of the chargeability of convex type at the vertex of which is the neighborhood of station 1700 can be seen.

6) Line Y (Fig. II-3-17)

The apparent resistivity shows from 62Ω·m to 1212 Ω·m value. The distribution of the apparent resistivity of more than 200 Ω·m is seen to the northwestern side from station 800, the depth of station 900, between station 1100 and 1300 and the depth of station 1700 . The part which shows the apparent resistivity of less than 100 Ω·m is seen between sta-

tion 900 and 1200 and these stations are the boundary of the apparent resistivity between the northwestern side and the southeastern side (same tendency with line W·X).

The chargeability shows the value from 1 to 34mV·sec/V. In the border from the shallowness of station 1600 to the depth of station 1400, the northwestern side becomes low chargeability and the southeastern side rather becomes the chargeability of the increasing. Also, between station 1700 and station 1900, high chargeability above 20mV·sec/V is shown.

7) Line Z (Fig. II-3-18)

The apparent resistivity shows from 122Ω·m to 1593 Ω·m value.
The distribution of the apparent resistivity of about 200 Ω·m is seen under about station 600 but the others become the apparent resistivity value of the increase for the most part.

The chargeability shows the value from 1 to 5mV·sec/V and that it is low severely over all lines .It doesn't sees IP abnormal area, too.

8) Apparent resistivity plan map (Fig. II-3-19)

The tendency which is common to each plan map from N=1 to 4 is that the high apparent resistivity zone of more than 200 Ω·m is distributed over the northwestern part of the area, the apparent resistivity zone of about 100 Ω·m is mainly distributed over the southeastern side. Also, looking at the center part of the area (station 900 - 1200 of line W·X·Y) of the N=1 plan figure, it is understood clearly about different tendency that the northwestern side shows the high apparent resistivity zone of about 1000 Ω·m, the central part shows the apparent resistivity zone of about 100 Ω·m, and the southeastern side shows an about 100Ω·m - 200 Ω·m value. It thinks that there is some discontinuing surface in the center part of the area.

When seeing the southeastern part, the low apparent resistivity zone of less than 100 Ω·m is distributed on the northern side of line A·B until it leads to N=4. Also, low apparent resistivity zone is observed in N=1 around the station of intersection of line A·B and line W, too, but the apparent resistivity zone becomes high as the depth increases (N becomes big).

9) Chargeability plan map (Fig. II-3-20)

As for the tendency which is common to each plan map from N=1 to 4, the high chargeability part which shows above 20mV·sec/V in the southeastern part of the area is seen but that only the distribution of the low chargeability part is seen about the area center to the northwestern part is given. A high chargeability part is divided into the part of the northeast of line A·B, and the part where line A·B and line W·X·Y intersects on the plan map of N=1. As for these two high chargeability parts, each shows high chargeability from N=1 to 4.

3-6-3 Analysis results of 2-D

1) Line A (Fig. II-3-21)

Generally, the resistivity is low and the low resistivity zone of less than roughly 100 Ω·m is distributed about the shallowness between station 300 and 400 and deeper than 200m

above the sea between station 500 and 900.

The chargeability shows more than roughly 20 mV·sec/V, high value over all lines. Especially, it makes the shallowness of the surface of the ground of station 300 and station 700 vertexes and the high chargeability continues to the depth.

2) Line B (Fig. II-3-22)

As for the southwestern side of the line, the resistivity of more than 200 Ω·m is seen, but the other part becomes the resistivity of the lowering and especially, as for deeper than 300m above the sea between station 400 and 900, the resistivity of less than roughly 100 Ω·m is distributed.

There are many parts which show a high value above 20mV·sec/V over all lines and the chargeability shows the tendency which is similar to A line. But, the depth becomes low chargeability from 100m above the sea between station 600 and 900.

3) Line C (Fig. II-3-23)

The resistivity value of less than 200 Ω·m is seen over the north of station 1100 , but as for the south of station 1100 , the high resistivity of more than roughly 1000 Ω·m is distributed. It thinks that some structure discontinuing surface exists in the station 1100 neighborhood from this thing.

The chargeability shows a value above 10mV·sec/V in the depth between station 1000 and 1300 but the others show a value below roughly 5 mV·sec/V.

4) Line W (Fig. II-3-24)

As it makes station 900 - 1100 a boundary , the high resistivity of more than roughly 200 Ω·m is distributed over the northwestern part of the line. Especially, the high resistivity zone of more than 1000 Ω·m is distributed over the shallowness between station 600 and 800. Incidentally, the distribution of the low resistivity of less than 200 Ω·m is seen to the shallowness between station 200 and 400. As for the southeastern part of the line, the high resistivity zone more than 200 Ω·m shows the depth between station 1200 and 1300,station 1600 and in the depth of the southeastern direction , but as for the others, the low resistivity zone of less than roughly 200 Ω·m is distributed.

The chargeability shows a value above 20mV·sec/V at the depth between station 1300 and 1500 and the shallowness between station 1600 and 1800 but the others show the low value of around 5 mV·sec/V roughly.

5) Line X (Fig. II-3-25)

As it makes station 900 - 1100 a border ,as for the northwestern part of the line, the resistivity zone of more than roughly 200 Ω·m is distributed. Especially, the high resistivity zone of more than 1000 Ω·m is distributed over the shallowness between station 400 and 800. As for the southeastern part of the line, the high resistivity zone of more than 200 Ω·m is distributed from the shallowness of station 1500 to the depth of station 1900 but as for the other part, the low resistivity of less than roughly 200 Ω·m is distributed. Especially, the

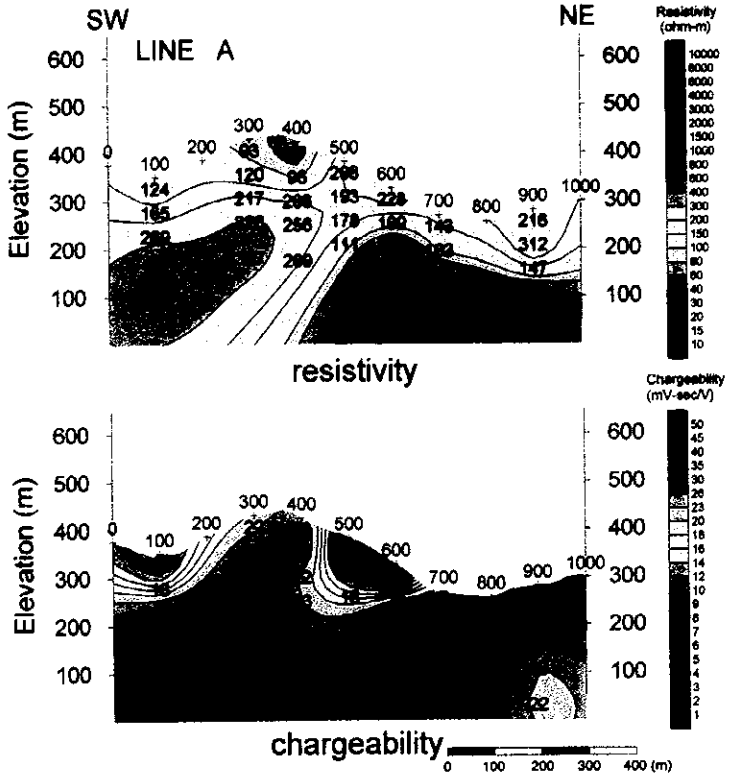

Fig.II-3-21 Results of model simulation of the I-4 area(A)

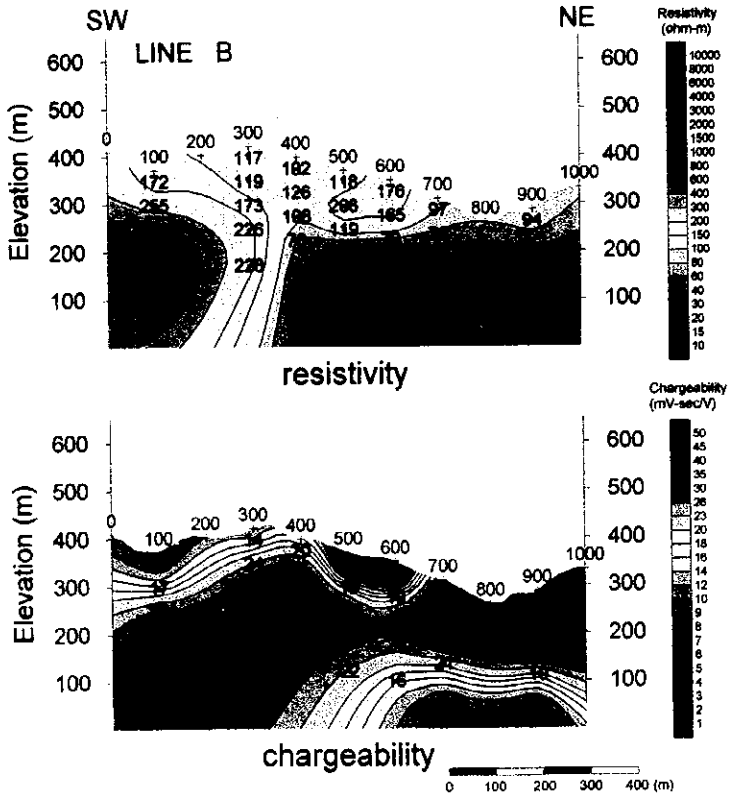

Fig.II-3-22 Results of model simulation of the I-4 area(B)

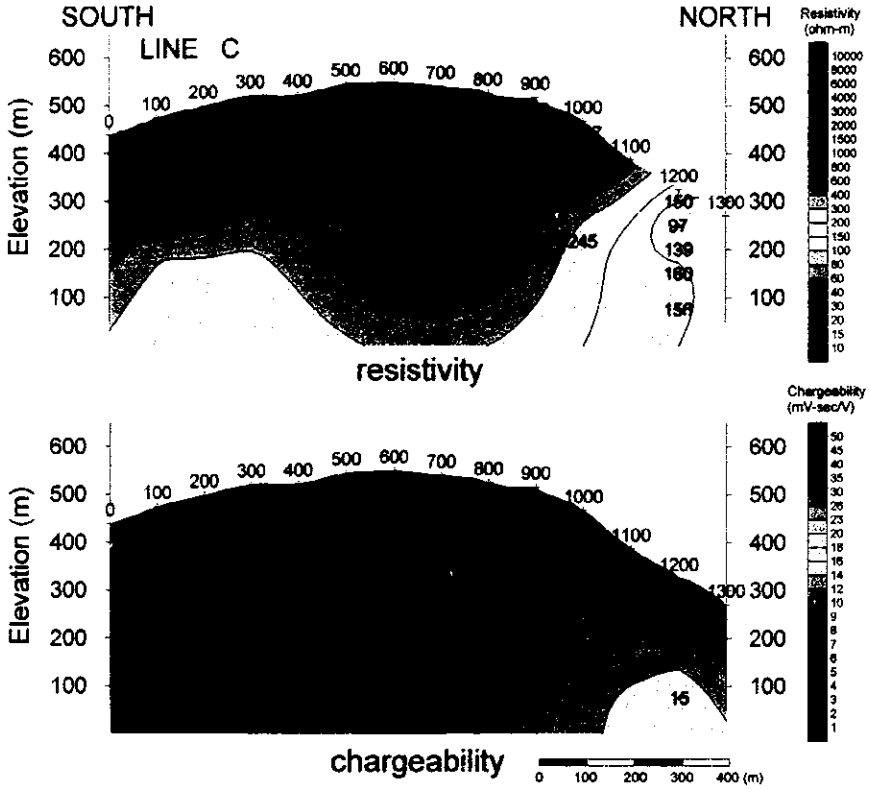

Fig.II-3-23 Results of model simulation of the I-4 area(C)

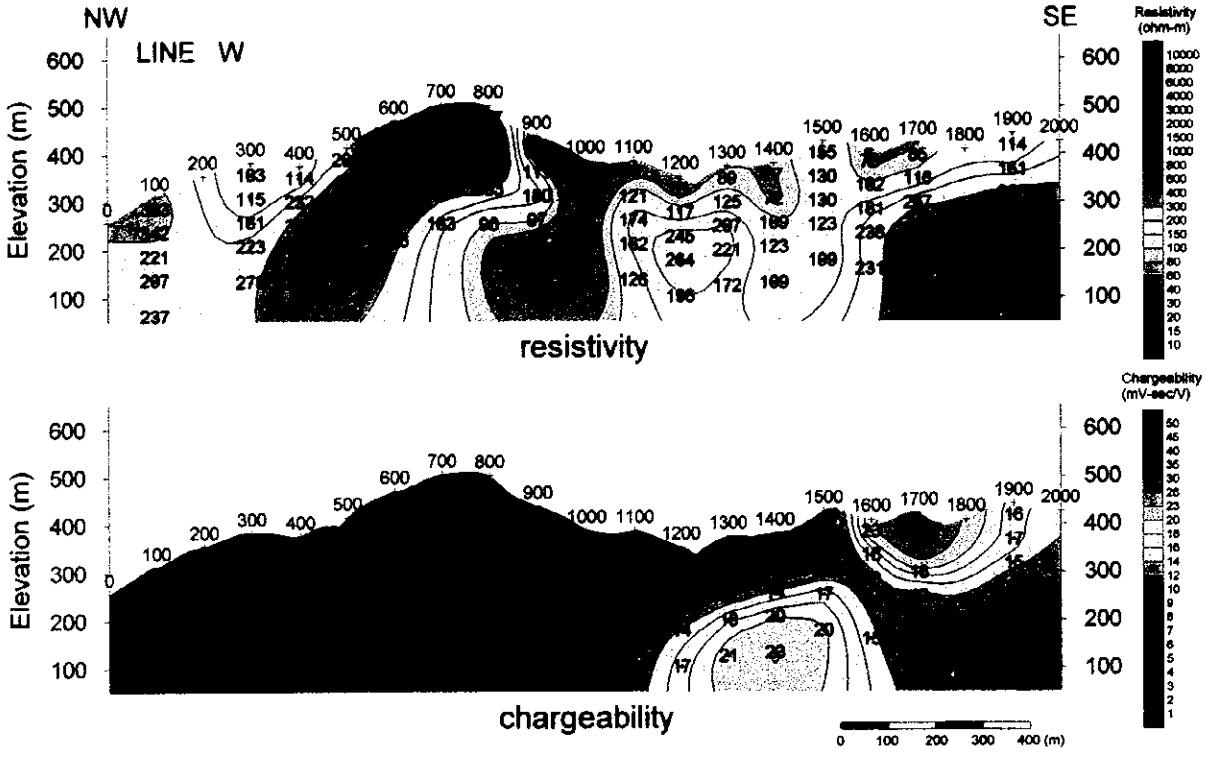

Fig.II-3-24 Results of model simulation of the I-4 area(W)

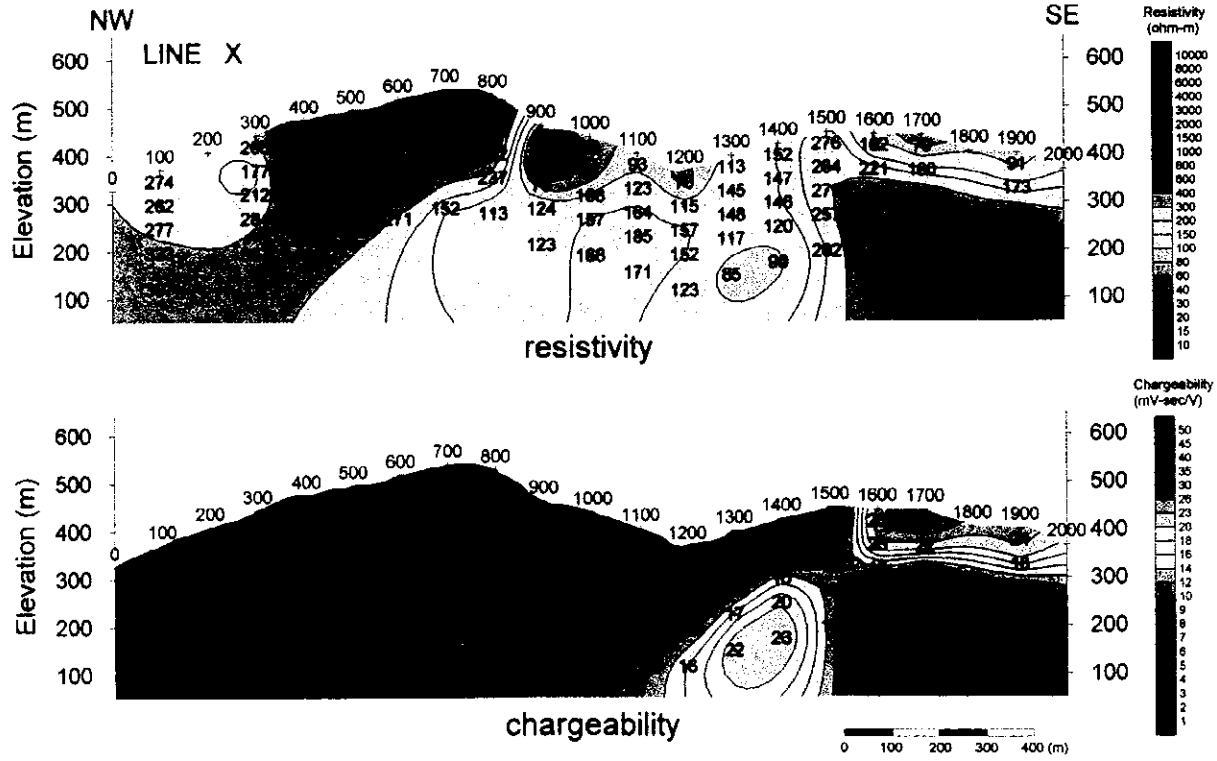

Fig.II-3-25 Results of model simulation of the I-4 area(X)

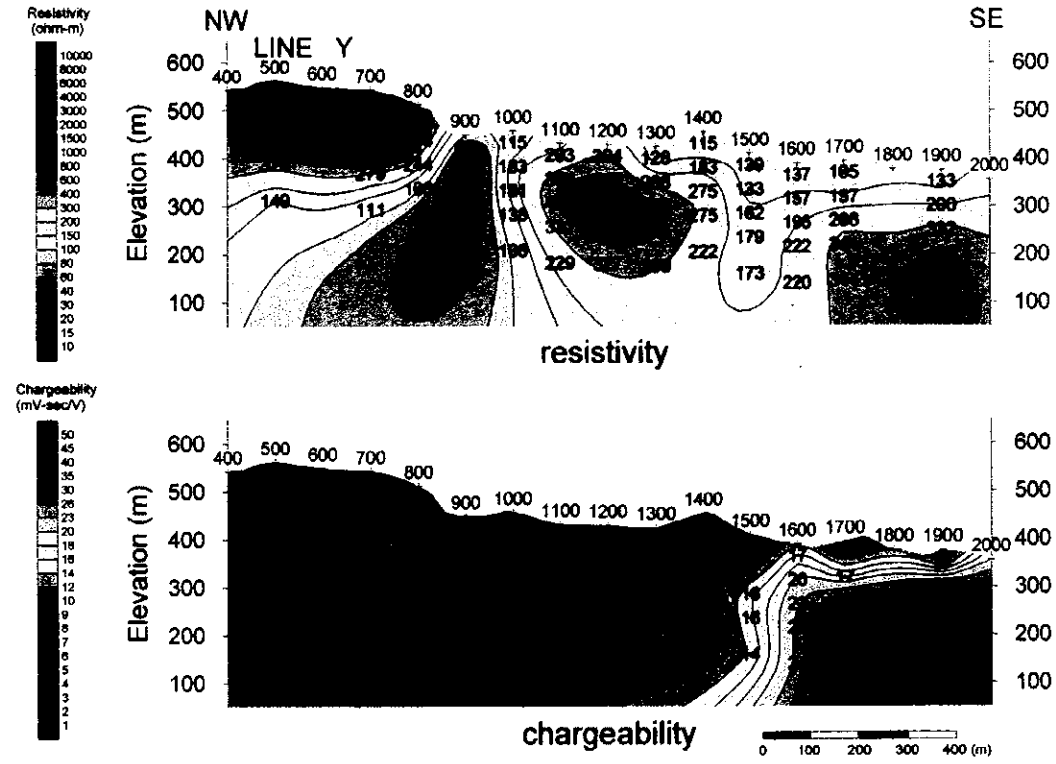

Fig.II-3-26 Results of model simulation of the I-4 area(Y)

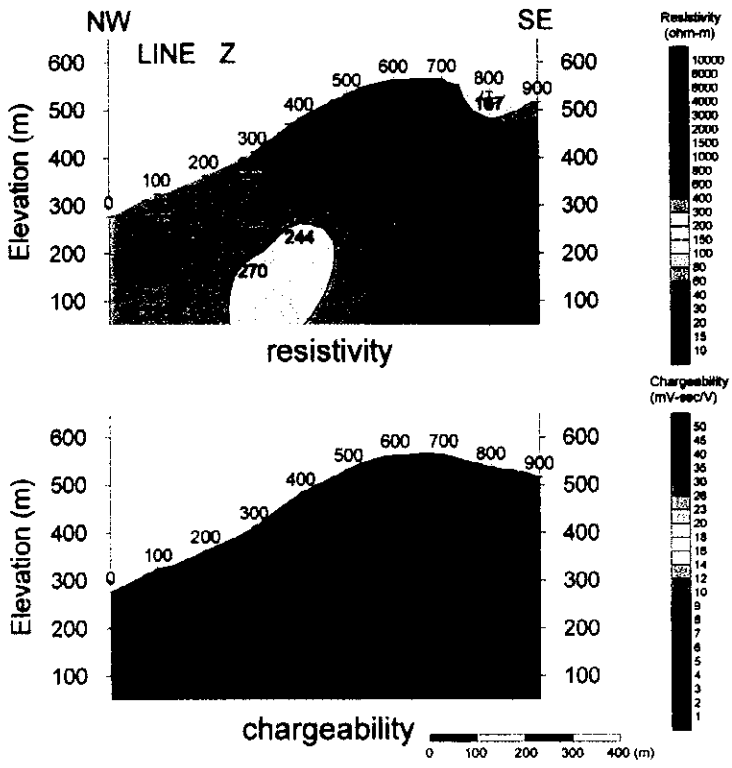

Fig.II-3-27 Results of model simulation of the I-4 area(Z)

low resistivity zone of less than 100 Ω·m is distributed over the shallowness between station 900 and 1200 and the shallowness of station 1700·1900.

The chargeability shows a value above 20mV·sec/V in the depth between station 1300 and 1400 and in the shallowness of the southeastern direction from 1600 but the others show a value below roughly 5 mV·sec/V.

6) Line Y (Fig. II -3-26)

The high resistivity zone of more than 200 Ω·m is distributed over the shallowness of the northwestern direction from station 800 ,the depth between station 1100 and 1400 and the depth of southeastern direction from 1600. The low resistivity zone of less than roughly 200 Ω·m is distributed over the other part and especially, the low resistivity zone of less than 100 Ω·m is distributed near station 900 to the depth.

The chargeability shows a value above 20mV·sec/V in deeper 300m above the sea in the southeastern direction from station 1600 but the others show a value below roughly 10 mV·sec/V.

7) Line Z (Fig. II -3-27)

The high resistivity zone of more than roughly 200Ω·m is distributed over whole line.

The chargeability shows a value below roughly 5 mV·sec/V and it doesn't see a conspicuous anomaly area.

3-6-4 Discussion

The apparent resistivity in this area is distributed from 26Ω·m to 4896Ω·m and the chargeability shows the high value of a maximum of 58 mV·sec/V. It extracted the part which shows the apparent resistivity of less than 100Ω·m and the high chargeability above 20mV·sec/V from the result of N=1 of the IP method measurement and indicated in Fig. II -3-28. Also, an ore bearing place and a fault were shown all together, pulling out from the geological map.

In this area, a fault is estimated on the north and on the central part. It is the fault which was estimated from the geological survey result that it displayed by the solid line in the map and it intersects with line W·X·Y. The fault in especially on the north is running near station 1100. As it makes station 1100 a border, the tendency is seen from the IP survey result that low resistivity zone is distributed over the southeastern part and high resistivity zone distributed over the northwestern part. It thinks that the high resistivity zone corresponds to limestone which is distributed over the northern area and the low resistivity zone corresponds to sandstone·shale or chert. On the southern side, the estimated fault is running around station 1200 but the resistivity tendency around this isn't changing into clearly like the fault on the northern side. Incidentally, it is in the discontinuation part of the resistivity zone which is seen around station 1100 of line C that it was shown by the dotted line in the map ,for the southern side shows high resistivity and for the northern side shows low

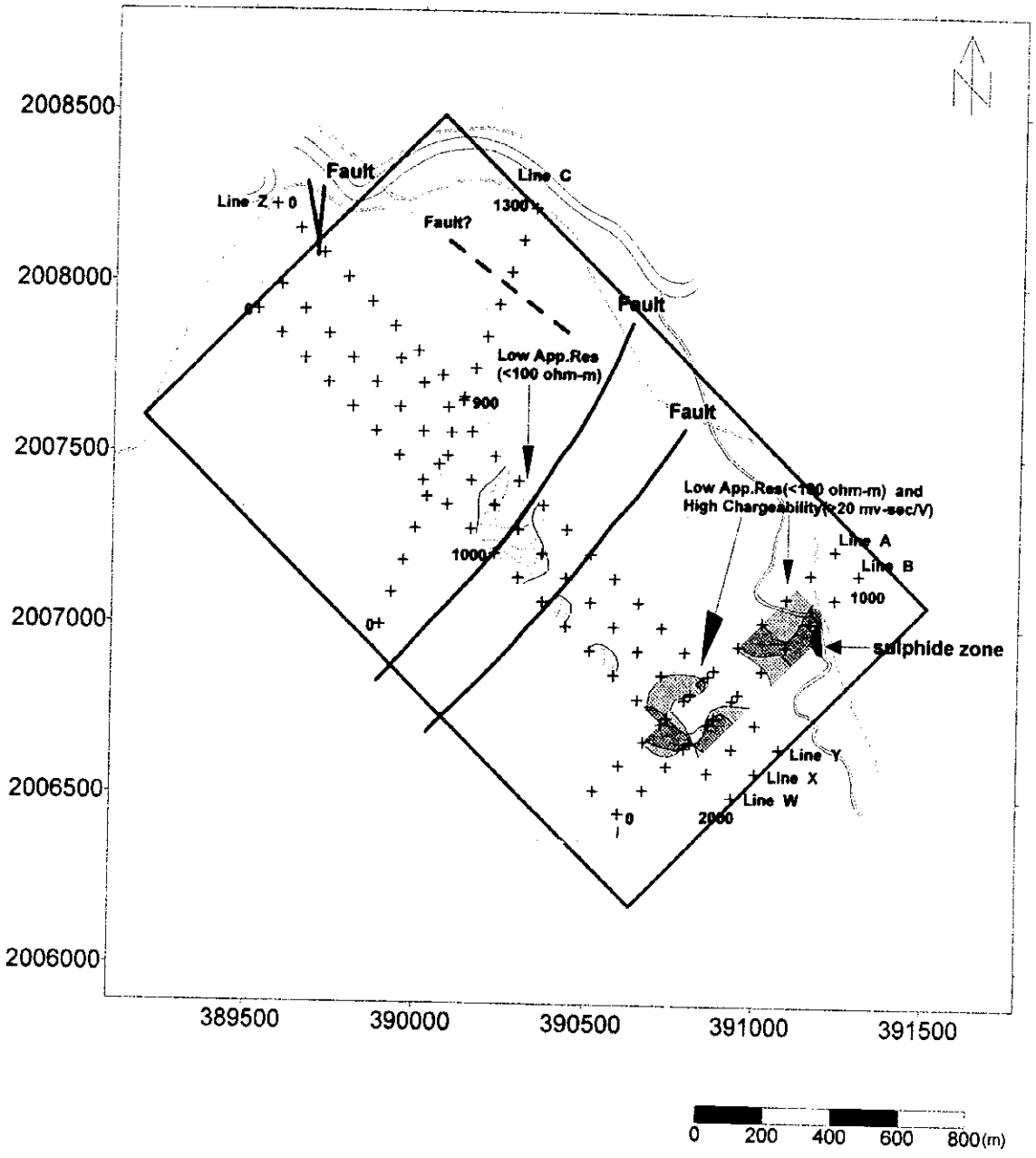

Fig.II-3-28 Integrated plan map of the I-4 area

resistivity.

Next, it examines about the southeastern part of the area where IP anomaly is seen.

As for the measurement result of line B and line A, the chargeability is very high approximately over all lines and the apparent resistivity is low ,about 100Ω·m.

An ore bearing place is seen in the neighborhood of station 800 of line B and the rock sample which was gathered around this shows high charging percentage. It thinks that these rocks contain either of galena and that they show high chargeability. When seeing the analysis result of 2-D, as for the resistivity in the southeastern part of line A·B, the deeper part of 200m above the sea is low with about 50Ω·m. The high chargeability seems to continue to the compared depth in line A from surface of the ground vicinity but it shows the tendency which chargeability becomes low in the deeper part of 100m above the sea in line B.

As for the part where line A·B and line W·X·Y intersect, the shallowness shows the apparent resistivity of about 100Ω·m and the chargeability shows about 30 mV·sec/V . When seeing the analysis result of 2-D , the western side from station 300 in line A·B shows the resistivity from 100Ω·m to 700Ω·m ,and the chargeability is about 30 mV·sec/V and results in continuing to the depth. Seeing the 2-D analysis result of line W·X, the chargeability of line A·B and the intersecting part is high chargeability till 300 m above the sea ,but in deeper part chargeability rather becomes low value . It thinks that this shows a thing with the strong tendency that the IP anomaly of the line intersection part is extended along line A·B . Furthermore in line W·X, in the part with the rather deep about 200m above the sea between station 1300 and 1400, the distribution (about 100Ω·m of resistivity) of the chargeability with 20 mV·sec/V is analyzed.

As the object of prospecting in the I-4 area, the neighborhood between station 500 and 800 of line A· B and the neighborhood of the intersecting area of line A·B and line W·X are given from above result. Especially, it thinks that about the neighborhood between station 500 and 800 of the line A and B suits a close prospecting because the anomaly area is wide and shallow from the results of 2-D analysis.

3-7 General consideration

The I-4 area can be divided into two blocks, northwestern part and southeastern part, by a fault in the NE - SW direction located in the central part of the area. The northwestern part consists of the Ordovician sedimentary rocks and the southeastern part consists of the Permian to Triassic sedimentary rocks.

The alternating beds of shale and sandstone with limestone lenses are occupied in the lower part. The upper part of the Ordovician sedimentary rocks is limestone in the northwestern part, respectively. The Ordovician rocks show a synclinal structure in the form of a ship bottom plunging on the north side.

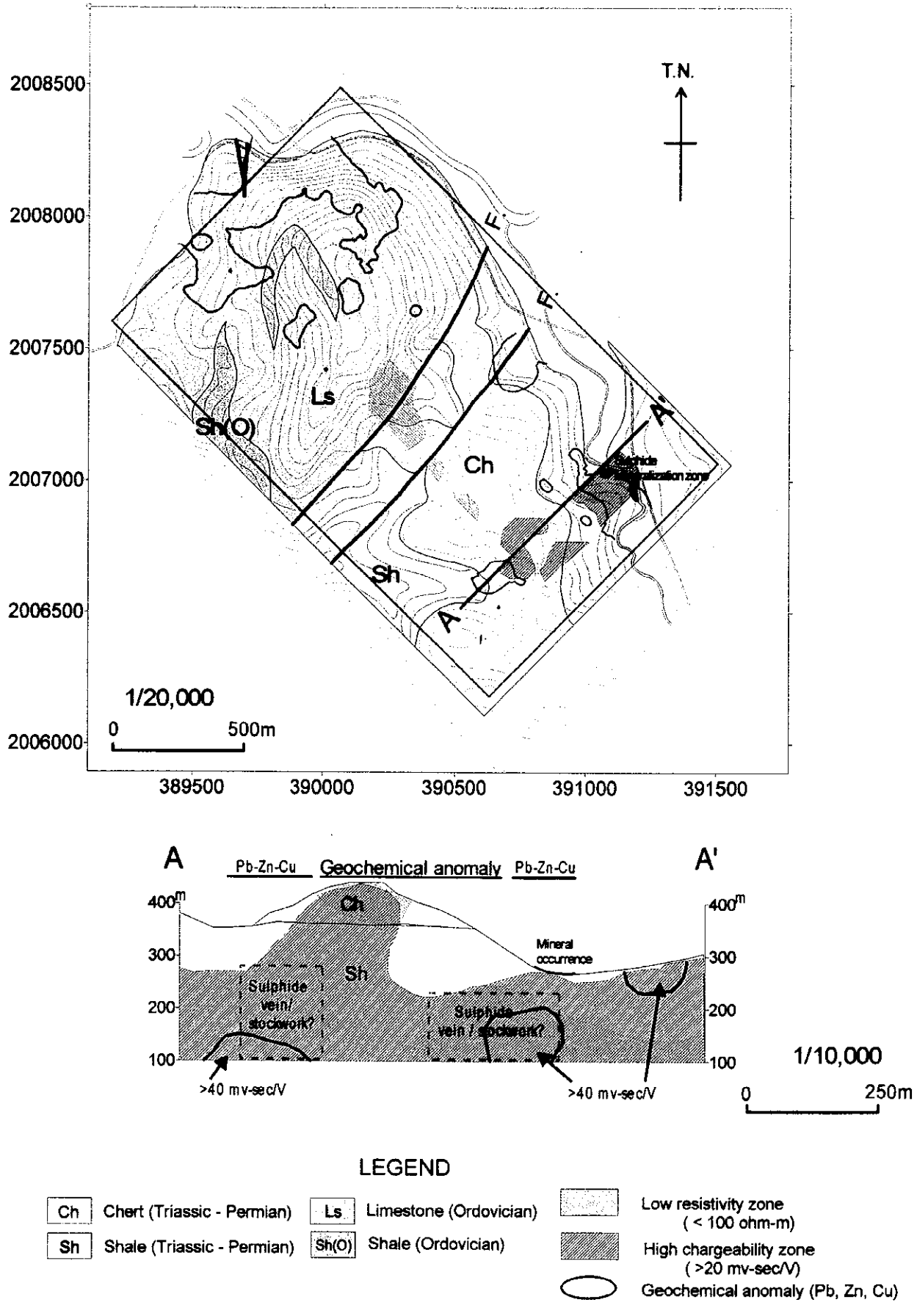

Fig. II-3-29 Interpretation map and profile of the I-4 area

The Permian to Triassic sedimentary rocks in the southeastern part consist of an alternating beds of black shale and sandstone intercalating limestone lens es in the lower part and a platy chert in the upper part. These rocks show a monoclinal structure with a northwest strike inclining toward the southwest.

Although a remarkable sign of mineralization is not observed in the limestone distribution area, small floats of gossan and floats of a quartz vein are found on a slope in the northwestern side of the mountain. There are also a lot of floats of a colorless idiomorphic calcite vein in this neighborhood. The geochemical survey revealed that geochemical anomaly of Zn, Pb, F, Sb, and As are distributed in a wide range in this area. The distribution of these geochemical anomalies seems to be predominated by a north - south system fault or fracture system. Particularly, a chargeability is low in correspondence with this high anomaly zone in the northwestern part of the area having high Zn anomaly like in the Dong Noi area. However, compared to its neighborhood, a relatively low resistivity area is observed. There probably indicate that this is a mineralized zone. The Zn anomaly is 200 to 1,000 ppm, which is lower by one digit than in the Dong Noi area. The characteristic of this area differs from that of the Dong Noi area in that the Zn anomaly is not accompanied by the Cd anomaly. Judging from the fact that this area has cracks and high F anomaly values, there is assumable that this is a halo of mineralization which formed fluorite deposits. In any case, since the distribution of the anomaly can be seen well from the urban area of Mae Sariang and is adjacent to the precincts of a temple, it is difficult to explore this ore deposit. However, since a mineralization like this was discovered in the Ordovician limestone, it is highly possible that other ore deposits exist in the same limestone layer up north from here.

Floats of barite, galena-quartz vein, and quartz vein are distributed here and there in the area covered by the Permian to Triassic sedimentary rocks. In addition, a lot of pyrite disseminations are observed in a chert layer along the national highway at the east end of the area.

Three or four several meter wide stockwork vein zones of galena-arsenopyrite are observed in an outcrop of strongly silicified shale extending over 70 m north and south along the banks of Nam Mae Ka Nai at the east end of the area. The vein stands steeply at N 45 to 50° W in the extension direction. Silicified rocks with pyrite dissemination are distributed on this extension about 100 m downstream.

Both geochemical survey and IP exploration show that geochemical anomaly of Pb, Zn, Cu, Ba, As, Sb, and Sn, low resistivity, and high chargeability zones are distributed in correspondence with its extension direction from this silicified rock outcrop. The geochemical anomaly zone also shows a stretch in the NW-SE direction that is the same as the direction of the vein observed in the outcrop. Judging from these facts, as shown in the model simulation cross sections of resistivity and chargeability, it is assumed that subsurface network veins are larger in scale than that observed in outcrop and exists as a high grade vein. The Pb and Zn

geochemical anomaly zones show the highest value and it is assumed that the center of the orebody is beneath survey points 600 to 700 along traverse line A where a high chargeability zone is distributed under the ground.

Similar geochemical and high chargeability anomaly zones show a directivity parallel to this mineralized zone and are distributed from the ridge on the southwest side from this zone to its west slope. It is thought that a zone equivalent in scale exists. However, unlike the mineralized zone in the eastern part, the lower part of this point shows a high resistivity.

Since there are a lot of similar small vein floats in the Mae Sariang area, it is likely that a vein type mineral showing like this is distributed on a small scale in various places. A possibility was also suggested that the geochemical anomaly in the Huai Pu - Huai Mae Pan areas which are adjacent to the south side of this area and have a similar geological environment is a vein type ore showing similar to this.

Chapter 4 Satellite Image Analysis

4-1 Processing of satellite image data

4-1-1 Data for satellite image analysis

In this study, satellite image analysis has been applied to a rectangle area extending 60km EW and 80km NS (white rectangle in Fig. II-4-1) using JERS-1/SAR and JERS-1/OPS image data. Mae Sarinag area of Thailand is locating at the center of the area for satellite image analysis that is covered by 4 scene of JERS-1 data (meshed part in Fig.II-4-1). Specification of each image is shown in Table II-4-1. Geographical map published by Thailand, 1/50000 in scale, has been used for a purpose of UTM projection of the satellite image.

Table II-4-1 List of satellite image data.

JERS-1/SAR		Obs. Date	Scene Center		Sun Angle		Cloud
Path	Raw	yyyy/mm/dd	North	East	Elev.	Azim.	(%)
132	270	1993/03/21	18:15	98:16	------	------	----------
132	271	1993/03/21	17:40	98:09	------	------	----------
133	270	1996/02/11	18:15	97:45	------	------	----------
133	271	1997/01/28	17:38	97:39	------	------	----------
JERS-1/OPS		Obs. Date	Scene Center		Sun Angle		Cloud
Path	Raw	yyyy/mm/dd	North	East	Elev.	Azim.	(%)
132	270	1993/02/12	18:15	98:26	51	144	< 1
132	271	1993/02/12	17:39	98:18	51	143	< 1
133	270	1996/01/05	18:14	97:55	45	155	< 1
133	271	1996/01/05	17:38	97:47	45	155	< 1

4-1-2 JERS-1/SAR

(1) Selection and acquisition of image data

Since JERS-1/SAR is a synthetic aperture radar (SAR), a type of side looking radar, it is not much influenced by the atmosphere, clouds or the sun. The requirements for selection of image data were that the scene in the same path must be of the same observation date and that the scene in the adjacent path must be of the consecutive observation date. However, there is no set of image data that satisfies these requirements.

The image data for path132/row270-271 satisfy these requirements. As the image data for path133/row270-271 do not satisfy these requirements, we have used image data of other observation date.

(2) Image processing

a) Correction processes

1) Noise reduction process

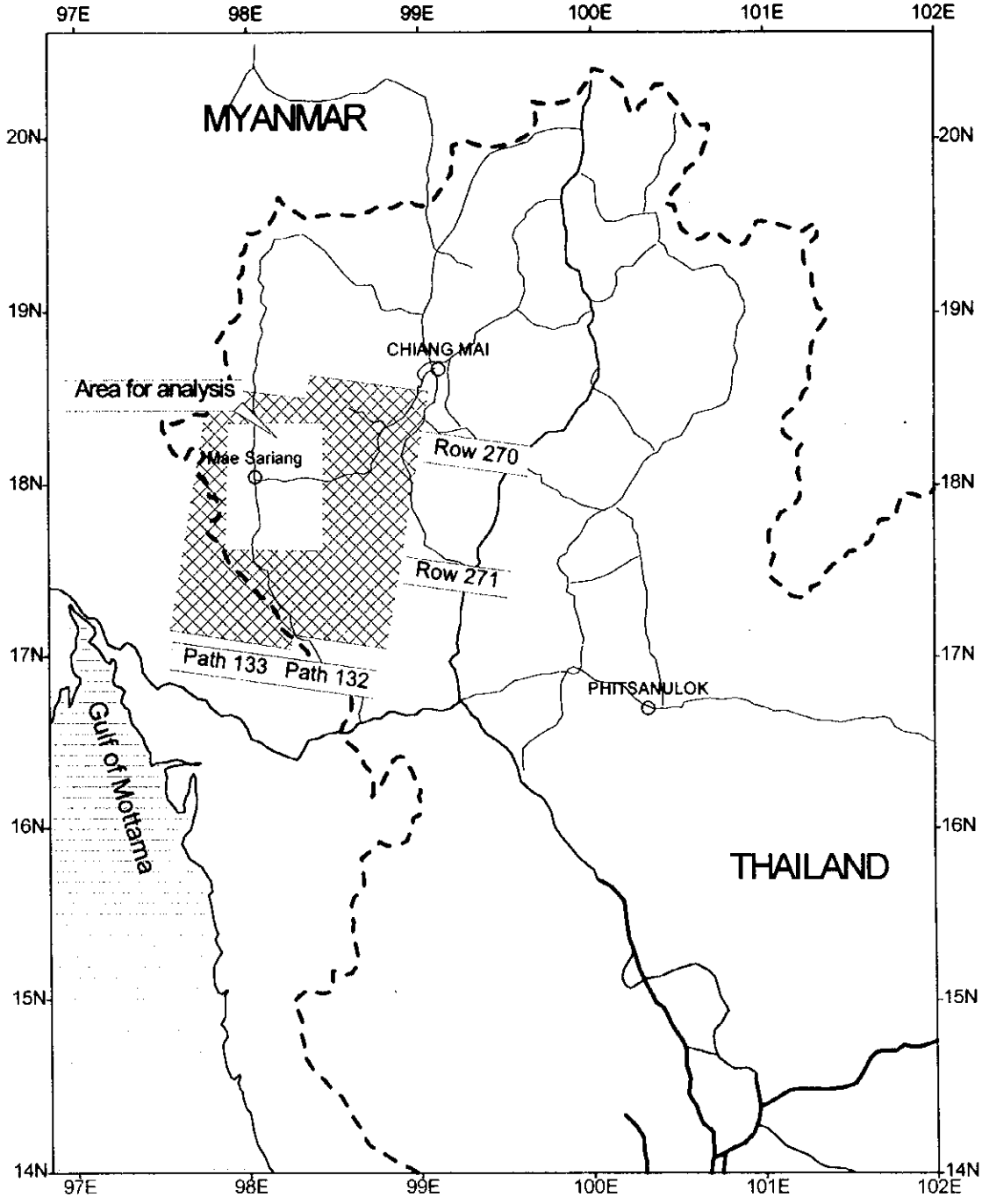

Fig. II-4-1 Coverage of JERS-1/SAR & OPS imagery and area for analysis.

Various types of noises that disturb analysis should be eliminated during preparation of images. Generally, the synthetic aperture radar (SAR) tends to include a larger amount of random noise than optical sensors. In this study, spatial filter (5 x 5 median filter) was applied for reducing random noise.

The gray level (DN : digital number) in JERS-1/SAR tends to show systematic shift in the upward/downward (east/west) direction. In a previous study for Southeast Asian area, correction was made using a sea area of Line1-6400/Sample2601-4000 at P083/R277. The gray level (DN*) in this sea area is approximated to:

$$DN^*(\text{line}) = 564.63 - 0.0837 \times \text{line} + 1.2055E\text{-}5 \times \text{line}^2$$

In this approximate expression, a minimum value (about 420) is present at the center. Using the above approximate expression and the minimum value, the gray level after correction (DN**) is:

$$DN^{**}(\text{line}) = DN(\text{line}) + 420 - DN^*(\text{line})$$

In this study, we have used this approximate expression.

2) UTM map projection

The JERS-1/SAR image data is basically projected in UTM. As these UTM coordinates are calculated from the satellite orbit information, they are not sufficiently accurate for the purpose of this analysis. In this study, UTM map projection has been carried out by mean of GCP method using topography maps (1:50,000) published by the Thailand.

3) Gray level adjustment and edge enhancement

In linear gray level adjustment, all area including both bright and dark parts in a JERS-1/SAR image can not be well displayed, as the gray level of the image data shows a distribution similar to Poisson distribution. In photo-geological analysis, it is preferable that the gray level is close to the gaussian distribution. In this study, to adjust the gray level (DN***) suitable for analysis, a logarithmic conversion of the gray level was made using the conversion formula:

$$DN^{***} = \ln(DN^{**}) \times 117 - 695$$

In addition, the edge was enhanced using the spatial filter (3 x 3 Laplacian). It is also necessary to enhance variation of topographical characteristics and lineament, because morphological expression is usually emphasized in photo-geological analysis.

b) Preparation of mosaic image

Using 4 scene images, the digital mosaic image data covering the entire study area was prepared (Fig. II-4-2). In principle, as the image data of each scene has already been projected with the UTM map, the mosaic image data can be generated by only arranging each image data on the UTM coordinates. However, a few pixels (dozens of meters) of offset may